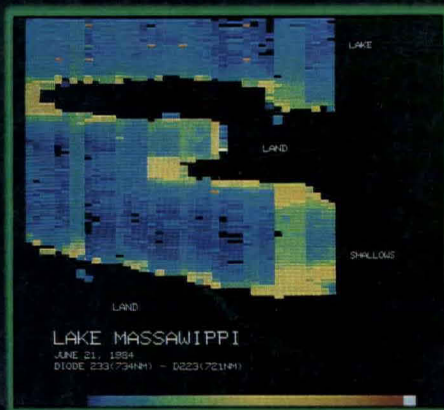


DFO - Library / MPO - Bibliothèque



12038951

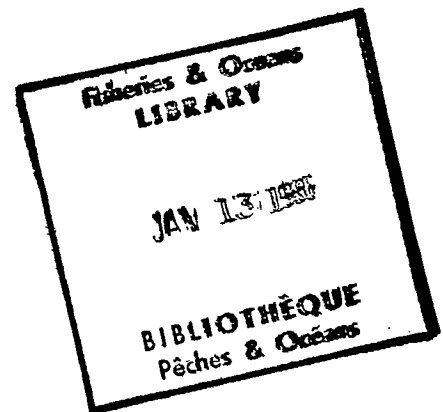


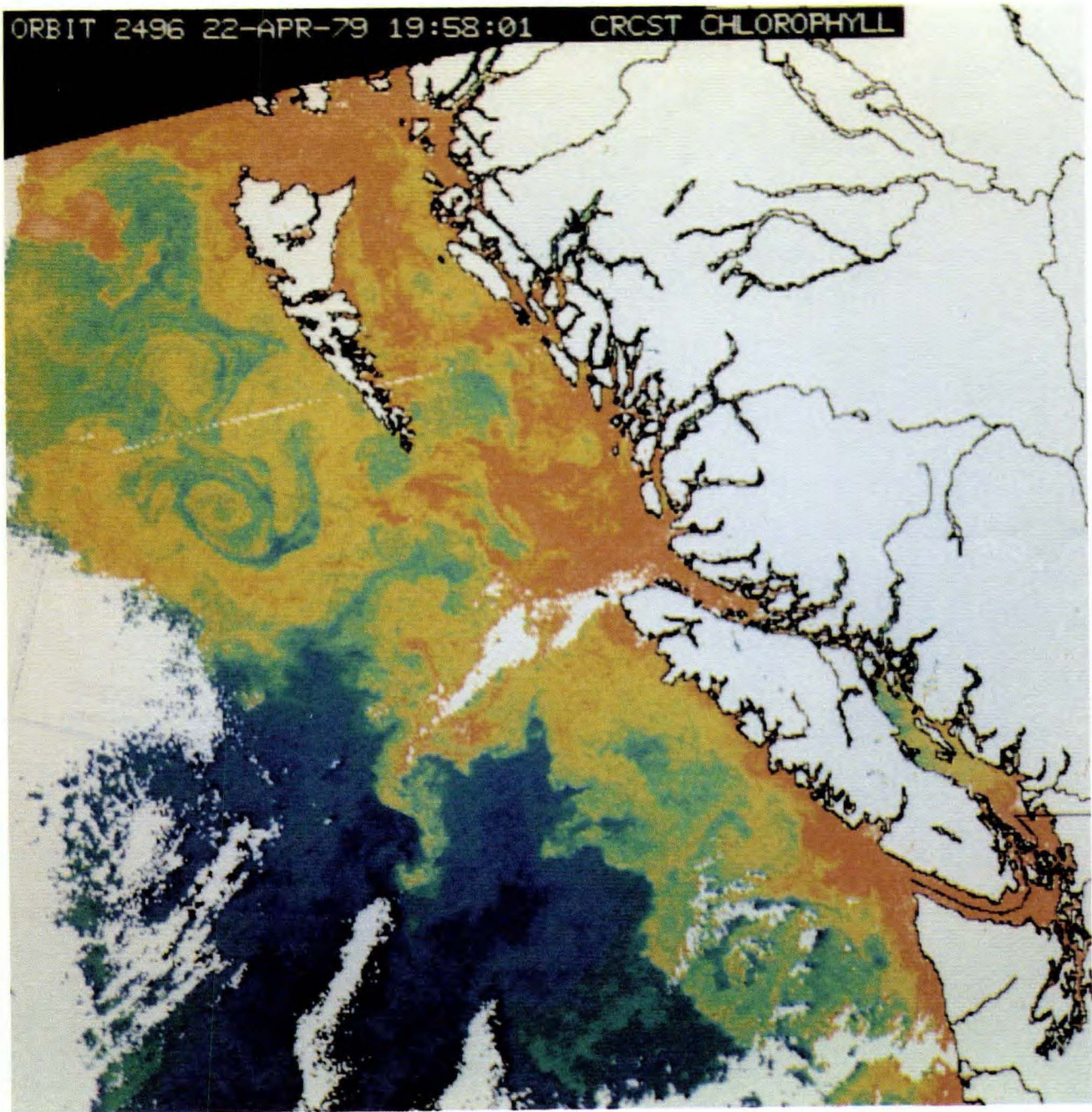
# Analysis of Test and Flight Data from the Fluorescence Line Imager

Gary A. Borstad  
H.R. Edel  
J.F.R. Gower  
Allan B. Hollinger

QL  
626  
C 314  
#83  
C.2

# **Analysis of Test and Flight Data from the Fluorescence Line Imager**





*Phytoplankton concentrations mapped optically by the Coastal Zone Colour Scanner from satellite. The data interpretation was provided by the Institute of Ocean Sciences, Sidney, B.C.*

# **Analysis of Test and Flight Data from the Fluorescence Line Imager**

**Gary A. Borstad**

*G.A. Borstad Associates Ltd.,  
10474 Resthaven Drive, Sidney, British Columbia V8L 3H7*

**H.R. Edel**

*Department of Fisheries and Oceans, Ocean Science Affairs Branch,  
200 Kent Street, Ottawa, Ontario K1A 0E6*

**J.F.R. Gower**

*Department of Fisheries and Oceans, Institute of Ocean Sciences,  
P.O. Box 6000, Sidney, British Columbia V8L 4B2*

**and Allan B. Hollinger**

*Moniteq Ltd., 630 Rivermede Road, Concord, Ontario L4K 1B6*



Published by

Fisheries  
and Oceans

Publié par

Pêches  
et Océans

Scientific Information  
and Publications Branch

Direction de l'information  
et des publications scientifiques

Ottawa K1A 0E6

©Minister of Supply and Services Canada 1985

Available from authorized bookstore agents, other bookstores  
or you may send your prepaid order to the  
Canadian Government Publishing Centre  
Supply and Services Canada, Ottawa, Ont. K1A 0S9.

Make cheques or money orders payable in Canadian funds  
to the Receiver General for Canada.

A deposit copy of this publication is also available  
for reference in public libraries across Canada.

Canada: \$6.00	Cat. No. Fs 41-31/83E
Other countries: \$7.20	ISBN 0-660-11960-9
	ISSN 0706-6481

*Price subject to change without notice*

Director and Editor-in-Chief: J. Watson, Ph.D.  
Publication Production Coordinator: G.J. Neville  
Typesetter: Graph Comp Design Ltd., Ottawa, Ont.  
Printer: K.G. Campbell Corporation, Ottawa, Ont.  
Cover Design: André, Gordon and Laundreth Inc., Ottawa, Ont.

Correct citation for this publication:

BORSTAD, G. A., H. R. EDEL, J. F. R. GOWER, AND A. B. HOLLINGER. 1985.  
Analysis of test and flight data from the Fluorescence Line Imager. Can. Spec.  
Publ. Fish. Aquat. Sci. 83: 38 p.

## Contents

ABSTRACT/RÉSUMÉ . . . . .	vii
EXECUTIVE SUMMARY . . . . .	viii
ACKNOWLEDGEMENTS . . . . .	viii
1. INTRODUCTION . . . . .	1
1.1. Description of the Fluorescence Line Imager . . . . .	1
1.2. Comparison with other sensors . . . . .	4
2. EVALUATION OF THE FLUORESCENCE LINE IMAGER INSTRUMENT PERFORMANCE . . . . .	6
2.1. Optical response . . . . .	6
2.2. Noise performance . . . . .	7
2.2.1. <i>Fixed pattern noise</i> . . . . .	7
2.2.2. <i>Random noise</i> . . . . .	9
2.2.3. <i>Other effects</i> . . . . .	10
2.3. CCD array non-uniformities . . . . .	10
2.3.1. <i>Linear effects</i> . . . . .	10
2.3.2. <i>Non-linear effects</i> . . . . .	11
2.4. Spatial and spectral resolution . . . . .	11
2.4.1. <i>Spatial resolution</i> . . . . .	11
2.4.2. <i>Spectral resolution and accuracy</i> . . . . .	11
2.4.3. <i>Spatial alignment of the FLI camera modules</i> . . . . .	11
2.5. Camera focus . . . . .	12
2.6. Optical "ghosting" . . . . .	12
3. CALIBRATION OF FLUORESCENCE LINE IMAGER DATA . . . . .	13
3.1. Calibration of the FLI arrays . . . . .	13
3.2. The IOS calibration routines . . . . .	13
4. EVALUATION OF THE CALIBRATION OF THE FLUORESCENCE LINE IMAGER . . . . .	15
4.1. Radiance calibration . . . . .	15
4.1.1. <i>Spectral radiance calibration</i> . . . . .	15
4.1.2. <i>Inter-camera errors</i> . . . . .	16
4.2. The uniformity correction . . . . .	17
4.2.1. <i>Spatial mode data</i> . . . . .	17
4.2.2. <i>Spectral mode data</i> . . . . .	17
4.2.3. <i>Effect of band formation on calibration of the FLI</i> . . . . .	17
5. EXAMPLES OF FLI IMAGE AND SPECTRAL DATA . . . . .	18
5.1. Swath width and foot print size . . . . .	18
5.2. Spectral data . . . . .	18
5.3. Spatial data . . . . .	23
6. CONCLUSIONS . . . . .	27
7. RECOMMENDATIONS . . . . .	29
8. REFERENCES . . . . .	31
APPENDIX — SUMMARY OF THE JUNE AND DECEMBER 1984 TEST FLIGHTS . . . . .	33
A.1. The June 1984 FLI operations staged out of Ottawa . . . . .	33
A.2. The December 1984 FLI operations in the Chesapeake Bay area . . . . .	33

## LIST OF ILLUSTRATIONS

Figure 1.	Conceptual summary of the FLI . . . . .	1
Figure 2.	Responsivity matrix for camera 2 . . . . .	6
Figure 3.	Spectral responsivity of cameras 2 to 5 . . . . .	6
Figure 4.	Responsivity variations across the spatial dimension of cameras 2-5 . . . . .	6
Figure 5.	Two-dimensional structure of the dark current offset (DARK.CAL;3) for camera 3 . . . . .	7
Figure 6.	Examples of dark data from the June flights . . . . .	7
Figure 7.	Comparison of dark data from the June 1984 flights and the January 1985 calibration . . . . .	8
Figure 8.	Analysis of signal-to-noise on data obtained in the laboratory and in the field . . . . .	9
Figure 9.	Departures from the mean responsivity on camera 5 . . . . .	10
Figure 11.	Example of a blemish on array number 3 . . . . .	10
Figure 11.	Grid patterns in the response of arrays number 1 and 2 . . . . .	11
Figure 12.	Altitude difference spectrum using data calibrated with the March 1984 calibration files . . . . .	15

## LIST OF ILLUSTRATIONS (*Continued*)

Figure 13.	Altitude difference spectrum using data calibrated with the January 1985 calibration files.	15
Figure 14.	Uncompensated gain variations between cameras in uniformity corrected imagery . . . . .	16
Figure 15.	Swath width and foot print size versus aircraft altitude for the December 1984 mission . .	18
Figure 16.	Upwelling, cloud "incident", and a calculated "reflectance" spectrum from off the Virginia coast, December 1984 . . . . .	18
Figure 17.	A family of upwelling spectra obtained over lakes in the Eastern Townships during June 1984 . . . . .	19
Figure 18.	Spectra obtained in the shallow water near the shores of Lake Massawippi showing an asymmetrical peak near 708 nm. . . . .	20
Figure 19.	Spatial distribution (spectral image) of the 708 nm peak in Lake Massawippi . . . . .	20
Figure 20.	Spectra obtained in shallow water near the shore of Lake Massawippi showing a progressive increase in near IR reflectance . . . . .	21
Figure 21.	Spatial distribution (spectral image) of the IR increase in Lake Massawippi . . . . .	21
Figure 22a.	Upwelling spectra from Pocomoke Sound and Chesapeake Bay . . . . .	21
Figure 22b.	"Reflectance" spectra from Pocomoke Sound and Chesapeake Bay . . . . .	21
Figure 23.	Variations of water colour indices along a flight-line over Pocomoke Sound and Chesapeake Bay, calculated from spectral data. . . . .	22
Figure 24.	Reflectance spectra of turbid waters of the Beaufort Sea obtained in 1983 with the IOS spectrometer. . . . .	22
Figure 25.	Difference spectra from line 7, Pocomoke Sound . . . . .	22
Figure 26.	Raw uncalibrated band 5 spatial imagery from the mouth of Chesapeake Bay . . . . .	23
Figure 27.	Uniformity corrected band 5 spatial imagery from the mouth of Chesapeake Bay. . . . .	23
Figure 28.	Uniformity corrected band 5 imagery with camera gain adjustments . . . . .	23
Figure 29.	Full resolution, uniformity corrected imagery from camera 2 band 5 compared to calibration data. . . . .	24
Figure 30.	Band 5 imagery with uniformity correction, camera gain adjustments and empirical atmospheric correction. . . . .	24
Figure 31.	Spectra from the region of the Chesapeake Bay bridge tunnel . . . . .	24
Figure 32.	Band 2 spatial imagery from the Winchester, Ontario agricultural area . . . . .	24
Figure 33.	Band 5 spatial imagery from over Norfolk, Virginia . . . . .	25
Figure 34a,b.	Colour composite taken over Renfrew, Ontario, July 1985 . . . . .	25
Figure 35a,b.	Edited colour composite, Renfrew, Ontario, July 1985. . . . .	26
Figure A.1.	Approximate position of lines 1 and 2, flown June 20, 1984 over northeastern Lake Ontario . . . . .	35
Figure A.2.	Approximate position of lines 3 to 13 and 15 over lakes in the Eastern Townships area of Quebec, June 21, 1984 . . . . .	36
Figure A.3.	Approximate position of spatial mode data obtained June 21, 1984 in transit over the Montreal area . . . . .	36
Figure A.4.	Approximate position of line 13 over the Petawawa Experimental Forest area, June 22, 1984. . . . .	37
Figure A.5.	Approximate position of line 14 over the Winchester, Ontario agricultural area, June 22, 1984. . . . .	37
Figure A.6.	Approximate position of lines flown on December 12, 1984 over Chesapeake Bay . . . . .	38
Figure A.7.	Approximate position of lines flown on December 13, 1984 over Chesapeake Bay . . . . .	38
Figure A.8.	Approximate position of line 2 flown on December 14, 1984 off Cap Hatteras, Virginia. .	38
Figure A.9.	Line 9 flown on December 15, 1984 at several different altitudes . . . . .	38

## LIST OF TABLES

Table 1.	Fluorescence Line Imager specifications. . . . .	1
Table 2.	Comparison of three basic types of sensors . . . . .	4
Table 3.	FLI system responsivity in spatial mode. . . . .	7
Table 4.	Camera gain adjustments for March 1984 calibration . . . . .	16
Table 5.	Camera gain adjustments for January 1985 calibration . . . . .	16
Table 6.	<i>In situ</i> data from Eastern Township Lakes, June 1984. . . . .	19
Table A.1.	Spatial mode band definitions for June and December 1984 test flights. . . . .	33
Table A.2.	Data summary for December 1984 flights . . . . .	34

## Abstract

BORSTAD, G. A., H. R. EDEL, J. F. R. GOWER, AND A. B. HOLLINGER. 1985. Analysis of test and flight data from the Fluorescence Line Imager. *Can. Spec. Publ. Fish. Aquat. Sci.* 83: 38 p.

This report describes the planning and analysis of test and flight data from the Department of Fisheries and Oceans Fluorescence Line Imager (FLI), a programmable imaging spectrometer designed for high sensitivity and high spectral resolution. Documents describing the package of computer programs written by Dawson Truax, that were used in the analysis, are also available.

As part of the work reported here, coordinated experiments of surface measurements were organized over a series of lakes, forests, and agricultural areas in southern Ontario and Quebec during June 1984 and in the Chesapeake Bay area of the eastern United States during December 1984. Data from these flights and some from laboratory tests conducted by J. F. R. Gower, Moniteq Ltd., and Itres Ltd. provided the basis for an evaluation of the performance of the sensor.

In this report, the FLI is briefly described and compared to other more conventional mechanical and solid state push-broom scanners. The relative advantages and disadvantages of each are outlined and the spectral imaging concept introduced. Data from the June and December missions and from laboratory experiments conducted by others is then analysed and discussed. The system responsivity, signal-to-noise ratio and spectral and spatial accuracy are analysed within the limits of the field data. Several types of noise and CCD array non-uniformities are documented and the calibration of the instrument discussed. Finally, examples of spectral and spatial image data from the two missions are presented and described.

## Résumé

BORSTAD, G. A., H. R. EDEL, J. F. R. GOWER, AND A. B. HOLLINGER. 1985. Analysis of test and flight data from the Fluorescence Line Imager. *Can. Spec. Publ. Fish. Aquat. Sci.* 83: 38 p.

Voici le rapport final d'un projet de planification et d'analyse de données d'essais et de vol obtenues avec l'imageur de la ligne de fluorescence (ILF) du ministère des Pêches et des Océans. L'appareil est un spectromètre imageur programmable de haute sensibilité et de haute résolution spectrale. Un rapport distinct contient les résumés des programmes et des imprimés des fichiers d'aide utilisés en direct avec le progiciel écrit par Dawson Truax.

Dans le cadre des travaux faisant l'objet du présent rapport, des expériences coordonnées de mesures de surface ont été menées sur une série de lacs, de forêts et de zones agricoles du sud de l'Ontario et du Québec en juin 1984 et dans la région de la baie Chesapeake, de l'est des États-Unis, en décembre 1984. Les données ainsi obtenues et quelques résultats d'essais de laboratoire menés par J. F. R. Gower, Moniteq Ltd. et Itres Ltd. ont servi de base pour une évaluation de la performance du capteur.

Dans le présent rapport, l'ILF est décrit brièvement et comparé à d'autres scanners plus classiques, en particulier à des scanners mécaniques et à des scanners en peigne à semi-conducteurs. Les avantages et inconvénients relatifs de chacun sont résumés et le principe de l'élaboration des images spectrales est exposé. Les données recueillies lors des missions de juin et de décembre ainsi que celles obtenues au laboratoire par d'autres chercheurs sont analysées et commentées. La réponse du système, son rapport signal/bruit ainsi que sa précision spectrale et spatiale sont analysés à partir de données de terrain. Plusieurs types de bruit ainsi que les écarts produits par la barrette CCD sont expliqués, de même que l'étalonnage de l'instrument. Enfin, des exemples d'images spectrales et spatiales obtenues lors des deux missions sont présentés et décrits.



## Executive Summary

The Fluorescence Line Imager was designed to provide high spectral and spatial resolution images of low radiance targets such as water, but with provision for imaging land targets with a lower sensitivity iris setting. The instrument has full software flexibility in spectral band definition in its push-broom imaging mode, and can also gather high resolution spectra in a "rake" spectrometer mode.

Most of the original goals of the instrument design have now been met. As well as producing spatial imagery similar to other devices currently in use (Fig. 29), the Fluorescence Line Imager has admirably demonstrated its flexibility by being reprogrammed several times to change the position and width of the spectral bands. It has a very wide dynamic range and has produced high spectral resolution data over both water and land targets (Fig. 16-23). This data has been used to create "spectral images" of very narrow spectral features which are not available from any other sensor currently in use.

The instrument has been used to collect data for forestry, agriculture, bathymetry and mariculture, as well as for the phytoplankton studies for which it was designed.

Fluorescence from the phytoplankton pigment chlorophyll *a* has been detected on water radiance spectra, in spite of interference from atmospheric absorption in the vicinity of the fluorescence line (Fig. 16). By normalizing FLI radiance spectra to the spectrum of the incident light, it has been possible to calculate pseudo-reflectance spectra identical to the reflectance spectra obtained in our past work with the Institute of Ocean Sciences (IOS) spectrometer. These FLI reflectance spectra also show a fluorescence line as a narrow peak in the vicinity of 685 nm.

The Fluorescence Line Imager has also enabled us to detect a previously undescribed spectral feature near 700 nm which may be usable for mapping benthic water plants (Fig. 18-21).

The instrument can probably now be considered operational, in spite of the fact that it is still a prototype. Most of the problems encountered were related to the fact that a "bread-board" instrument was not built first and faults or inadequacies had to be discovered through operational testing. Work on the instrument since its delivery has improved its performance considerably, and the collective experience with the instrument and the data it produces, has shown that further improvement can be expected.

The high spectral resolution and extreme flexibility give the FLI a very significant advantage over other instruments available today. It is now important that the technical lead and momentum generated by the FLI program should not be lost. Various technical improvements suggested by this work should be investigated and work should be started on a space version of the instrument.

## Acknowledgements

The help of many people must be acknowledged in making this work possible. At the most fundamental level we thank the senior staff of DFO and of the Interdepartmental Committee on Space who found the funds to design and construct the FLI imaging spectrometer, and to carry out this evaluation. Staff of Moniteq Ltd. (Toronto) and Itres Ltd. (Calgary) carried out the design and construction. L. Gray and J. Harron of Moniteq Ltd. were helpful during the field operations, and along with Dr. C. Anger, B. Green and S. Babey of Itres Ltd. also gave useful advice and assistance. The Canada Centre for Remote Sensing (CCRS) staff and aircrew were extremely cooperative in assisting with the instrument's installation in their aircraft, and in arranging flight operations. Dr. Kalff and Chambers and the students at the McGill University field station, Lake Memphramagog, Quebec collected *in situ* samples in conjunction with the June 1984 flights. D. Truax (Apocalypse Enterprises Ltd.) wrote all of the specialised computer programs to analyse the FLI data on the IOS image processor. He also provided assistance with the interpretation of the data and together with J. Wallace (DFO), kept the image processor alive during the course of the data analysis. J. Wallace also provided technical assistance and advice regarding the FLI.

# 1. INTRODUCTION

The Fluorescence Line Imager was designed specifically for the Department of Fisheries and Oceans, to image the water spectral reflectance changes caused by different phytoplankton concentrations in the near-surface layer of the sea. However, a change of iris setting allows collection of reflectance data over land, with parameters suitable for studies in a wide variety of fields, and with spectral capabilities that give it advantages over any other instrument available today.

The mapping of phytoplankton distribution and growth has important applications in fisheries and physical oceanographic studies. Phytoplankton constitute the first link in marine food webs and, along with benthic plants, are the only significant organisms in the marine and fresh water which convert solar energy into organic biomass. The ability to rapidly and repeatedly monitor their changing distribution and abundance on local or regional scales would be a major step towards understanding phytoplankton ecology, organic production at higher trophic levels, and the ecological effects of man's activities in lakes and coastal waters.

The light absorbing pigments collectively known as chlorophyll *a* (hereafter referred to as chlorophyll) are commonly used by oceanographers and limnologists as an index of phytoplankton abundance. In standard practice the pigment is extracted and measured in solvent by absorption spectroscopy or fluorometry (Strickland and Parsons 1972).

In fact the strong absorption of blue light by chlorophyll is responsible for the apparent colour changes of water bodies as the phytoplankton concentration increases and this phenomenon has recently been exploited to enable remote sensing of the pigment from aircraft and satellites (Clarke et al. 1970; Arvesen et al. 1973; Morel and Prieur 1977; Gordon et al. 1983; and many others). See cover for sample image.

A second independent method for remote detection of chlorophyll has been developed at the Institute of Ocean Sciences by Gower and his co-workers (Neville and Gower 1977; Gower 1980; Gower and Borstad 1981; Brown and Borstad 1982; Borstad and Gower 1984; Gower et al. 1984). This work has shown that *in vivo* fluorescence by the plant pigment chlorophyll *a*, stimulated by direct or scattered sunlight, provides a distinctive signature for the presence of this phytoplankton pigment in near surface water. The method has been used with success in several mapping exercises in the Canadian Arctic (Borstad and Gower 1984; Borstad 1985), off British Columbia (Borstad et al. 1980; Borstad et al. 1981) and in Europe (Gower and Borstad, unpublished data). Applications include studies of the distribution of Pacific salmon and the ecology of the endangered bowhead whale.

Interpretation of water colour is also important for hydrographic mapping. Algorithms have been developed (Lyzenga 1978; Lyzenga et al. 1979; Jain et al. 1982) for the determination of water depth, bottom features and water quality. Applications of passive multispectral remote sensing are being considered for engineering surveys.

The mapping of mineral deposits is another area of application of multispectral imaging. The laboratory spectra of a wide variety of minerals (Hunt et al. 1973) provide a basis for the remote sensing of mineral outcroppings (Vincent 1972; Schmidt 1976). Minerals affect foliage reflectance through heavy-metal poisoning (Lyon 1975; Bolviken 1977).

Collins (1982) has examined the chlorophyll red edge in reflectance spectra, to identify geochemically stressed vegetation using an airborne spectrometer.

In 1980, the Department of Fisheries and Oceans commissioned a study by the Canadian Corporation for University Space Science (CCUSS) to investigate the "feasibility of mapping chlorophyll fluorescence from space". This study (CCUSS 1981) concluded that it was within the current technical capabilities to build an imaging spectrometer with sufficient spectral and spatial resolution to image chlorophyll fluorescence from spacecraft altitudes. Consequently, a contract was let to Moniteq Ltd. of Toronto with subcontract to Itres Ltd. of Calgary to design and build "a CCD imaging spectrograph to measure chlorophyll from a high altitude aircraft". The Fluorescence Line Imager (FLI) was delivered in May 1984 and has now been flown on four test flights.

This report is an edited version of the final report submitted by G. A. Borstad Associates Ltd. under DSS contract No. 06SB.FP941-4-0393 for the planning and analysis of test and flight data from the Fluorescence Line Imager. It summarizes the results and analyses of some of the data from flights in June and December 1984. It also reviews the results of technical improvements and modifications carried out under DSS contracts 06SB.FP941-4-1110, -2481, and -3630. One example is also presented of image data from the latest series of test flights in July 1985.

The report comprises: (1) A description and evaluation of the FLI from test data acquired on the above two test flights and in laboratory calibrations performed by J.F.R. Gower, Itres Ltd. and Moniteq Ltd.; (2) A comparison of the FLI with more conventional mechanical and push-broom scanners operated by the Canada Centre for Remote Sensing (CCRS); and (3) Examples of data from these two test flights, illustrating the data obtained by the FLI and demonstrating uses of the FLI for environmental research.

## 1.1. Description of the Fluorescence Line Imager

The Fluorescence Line Imager uses as its sensing elements five CCD (Charge Coupled Device) Frame Transfer Arrays manufactured by the English Electric Valve Company of London, England. These are two dimensional arrays of light sensitive silicon diodes, on which the charge at each diode can be transferred to the neighbouring diode (and therefore by sequential transfers, off the array) by application of external control signals. In the FLI, the arrays are mounted in five separate camera modules and each is illuminated so that across-track spatial information falls along their long dimension (385 elements), while spectral information for each spatial pixel registers across the shorter (288) dimension (Fig. 1). The combined arrays provide spectral resolution of 2.5 nm over the range 430 to 800 nm and across-track spatial information in the form of a 1925 element push-broom array. Table 1 summarizes the instrument specifications.

Like many other state-of-the-art remote sensing devices, the FLI can perform high spatial resolution mapping (in "spatial mode") by forming push-broom images in 8 bands. However, unlike other systems in use today, the placement

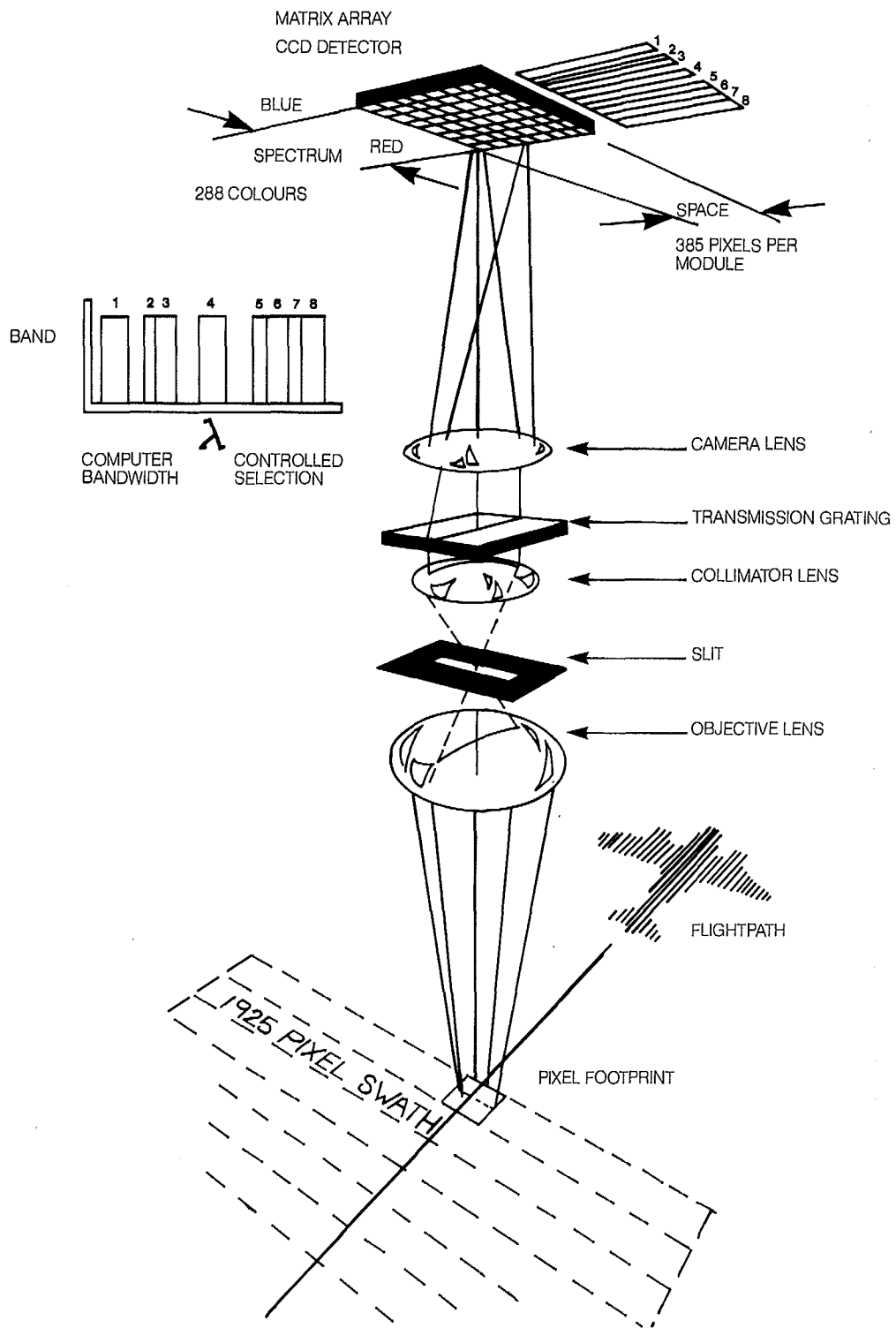


FIG. 1. A conceptual diagram of the DFO Fluorescence Line Imager (from Moniteq 1984b).

and width of FLI spectral bands are selectable through computer software in steps of 1.4 nm.

In "spectral mode", the device can also operate as 40 spectrometers, each with resolution of 2.5 nm. In this mode it can also be thought of as a low spatial resolution, 40 element push-broom scanner with 288 spectral bands. The location and width of the footprint of each spectrometer can be selected with the same algorithm that forms spectral bands in spatial mode. In practice these footprints are chosen to be separated in space across the FLI's field of view, and cover the

ground like the tines on a garden rake. We use the name "rake spectrometer" for this mode.

## 1.2. Comparison with other sensors

The relative advantages of push-broom scanners such as the MEIS II (Multiple-detector Electro-optical Imaging Sensor) and the FLI compared to more conventional mechanical scanners such as the Daedalus MSS (Multi Spectral Scanner) have been discussed by Slater 1980; Till et al. 1983; Neville et al. 1983; McColl et al. 1983; Norwood and Lansing 1984 and

TABLE 1. Fluorescence Line Imager specifications.

Spectral:	coverage	430 to 800 nm
	number of pixels	288
	pixel size	1.4 nm
	resolution	2.5 nm
Spatial:	coverage	~70 degrees with five cameras
	number of pixels	1925
	pixel size	0.65 mrad
	resolution	1.3 mrad
Modes	spatial	8 bands are formed from spectral pixels. Choice of pixels is under software control. A push-broom image 1925 pixels wide is formed in each band.
	spectral	spectra covering 430 to 800 nm with 2.5 nm resolution are recorded from 40 different directions across the swath (8 per camera). Choice of direction and number of elements per band is under software control (slow mode) or is fixed with 2 elements per band (fast mode).
Sensitivity		maximum 1900:1 S/N for a band of 16 detector elements at full scale signal which is set to near ambient light levels over water.
Integration times		40 ms minimum, 90 ms (spatial), 150 ms (spectral) typical
Digitization		12 bits on chip, summation to 16 bits after readout
Detector type		five 385 × 288 element EEV P8600 arrays
Optics		Transmission grating with F1.4 Nikon lenses
Aircraft mountings		RC-10 compatible mount in DC-3 and Falcon Fanjet
Data recording		Bell and Howell 14 track HDDT 8 × 875 kbit.s <sup>-1</sup> recorded
Weights	Head	70 kg
	Data acquisition	26 kg
	Thermal unit	41 kg
	(tape recorder not included, no real-time display at present)	
Size	Head	66 × 48 × 38 cm
	Data acquisition	48 × 35 × 60 cm
	Thermal unit	38 × 42 × 54 cm
Power	Head and acquisition	450 W
	Thermal cooling unit	Up to 1 kW

others. Table 2 summarizes and compares some of the characteristics of the three types of sensors.

The major difference between mechanical scanners and push-broom sensors is the number of detector elements. Scanners such as the Daedalus MSS usually have from two to twelve silicon diode detectors, with spectral selection either by a prism spectrometer or by filters. The MEIS II uses eight linear CCD arrays, each with 1728 elements, also with spectral selection by filters installed in front of the arrays. The Fluorescence Line Imager is the next evolutionary step, with five two-dimensional CCD  $288 \times 385$  element arrays. Spectral selection in the FLI is by dispersion of the incoming radiance across the second, along-track dimension of the array.

Mechanical multi-spectral scanners generally employ a rotating mirror to sweep the field-of-view of a few detectors across the scene, thereby effectively presenting any one point on the far-field to the detector for a short period determined by the speed of mirror rotation and the imaged swath. The increase in detector number in push-broom sensors allows much longer integration times since each detector can view the far-field over as long a period of time as it takes the platform to move the distance in the scene corresponding to the instantaneous field of view. This longer dwell time for each detector leads to higher signal-to-noise ratios than in mechanical sensors and this in turn permits imaging of narrower spectral bands or of darker, lower radiance targets such as water.

The geometry of mechanical and pushbroom sensors are also significantly different. Whereas scanners require complicated correction for scan mirror velocity, image skew caused by the relative motion of the scan and the sensor and spectral band offsets, pushbroom devices view the entire swath simultaneously with relatively simple geometry. Both the MEIS II and FLI use several separate arrays which must be physically aligned to produce co-registered imagery. In the MEIS II, the geometry of the 5 channels is fixed by the construction of the camera head, but the geometric accuracy with which images can be produced depends on very precise characterization of each filter set. The FLI does not have changable filters, but the design of the prototype instrument necessitates realignment of the 5 separate camera modules each time the system is taken apart for maintenance or repair.

The trend in remote sensor design has been towards more and narrower spectral bands and greater spatial resolution as the technology of data recording and handling improve. Object plane mechanical scanners now represent a mature technology and the best can at present obtain very high geometric accuracy on the order of 0.001 mrad (Norwood and Lansing 1983). Those in civilian use are much less accurate, however. The Daedalus/MDA DS1260 Multi Spectral Scanner currently operated by CCRS as an airborne system (Zwick et al. 1980) has an instantaneous field of view of only 2.5 mrad. By comparison, the MEIS II and FLI can presently obtain 0.7 and 0.8 mrad, respectively, about three times better than the Daedalus MSS and about the same as the Coastal Zone Colour Scanner (0.65 mrad). Since this resolution is near that commonly available at present, it will probably be acceptable for airborne imaging over land and for low spatial imaging of water features from space. This resolution is however, significantly less than the Thematic Mapper on LANDSAT 5 (0.043 mrad) or the HRV to be launched on the French SPOT (0.012 mrad). If the current high demand for LANDSAT 5 data and the great attention being directed at SPOT is an indication, sensors being launched in the 1990's will require high spatial resolution in order to be competitive for use over land targets.

The trend to higher spectral sensitivity is also illustrated by comparing the MSS, MEIS II, and FLI. The spectral resolution of the Daedalus /MDA Multispectral Scanner is determined by transmission filters and varies from 30 to 200 nm across the visible region. Because of a  $100 \times$  increase in sensitivity and decrease in noise, the MEIS II is capable of a significant increase in spectral resolution over mechanical scanners (Till et al. 1983). Spectral band selection is relatively easy, through exchange of transmission filters. Most operations have been with band passes simulating other sensors, however data has been obtained with 2-3 nm wide bands.

The FLI is also a push-broom sensor using charge coupled devices, and in that respect is similar to the MEIS II, but the use of two-dimensional arrays and diffraction gratings in the FLI provides a spectral capability not possible in any device using filters. All wavelengths between 430 and 800 nm are accessible to the FLI, in steps of 1.4 nm. Band width and placement are defined under software control. As a result, bands can be notched to avoid spectral absorption features

TABLE 2. Comparison of three basic sensor types.

	Mechanical scanners (Daedalus MSS)	Linear arrays (MEIS II)	2-D arrays (FLI)
Optics	on-axis	...wide angle, one dimension...	
Number of detectors	10	~15 000	~550 000
Sensitivity	limited by short dwell time	...much longer dwell times...	
Radiometric calibration	relatively simple	more difficult	most difficult
Flexibility	limited by hardware	spectral bands selected by changing filters	bands selected through software

and easily changed during flight. A current data handling limitation restricts operation of the FLI to recording 8 bands, but this will probably increase as technology improves.

As will be discussed in section 5, the FLI has now been demonstrated in both operating modes. The spatial mode provides data not unlike other sensors, however the spectral mode data is unique. As well as providing high spectral resolution which has already allowed detection of small spectral features previously unsuspected, it is also possible to use the system as a low spatial resolution 40 element pushbroom scanner with 288 bands to form images of spectral features as narrow as 2.5 nm. This "spectral imaging" capability has permitted us to map the extent of an undescribed spectral phenomenon related to the red reflectance of benthic plants in lakes. When real-time data processing and display is added to the system, it will theoretically be possible to detect these spectral features using the high spectral resolution spectral mode, redefine the spatial mode bands optimal for that feature and then map the geographic extent of the feature with high spatial resolution, all on the same flight.

This flexibility will be one of the major advantages of the Fluorescence Line Imager, since a satellite borne FLI-like sensor could be easily re-configured in flight for many very different tasks. The civilian sensors currently aloft or due to be launched have relatively wide and fixed spectral bands. They all represent a compromise between the demands of user groups, usually with the result that the configuration is not optimal for anyone. Because of the generally conflicting requirements for spatial and spectral resolution and time of image acquisition, there has been a recommendation from the user community to design and operate future systems with a single application in mind (Slater 1980). A programmable imaging spectrometer such as the FLI could meet the require-

ments for different spectral and spatial resolution and could be reprogrammed on consecutive orbits.

The major disadvantage of push-broom sensors is related to the increase in number of detectors. The evolution from 10 to 14,000 to 500,000 separate detector elements represents an enormous increase in spectral resolution, flexibility and in signal-to-noise performance, but it is at the cost of a significant increase in the calibration difficulty and in the data processing burden. The FLI represents an extreme in the evolution towards multi-detector sensors. One of the problems foreseen in the CCUSS report (CCUSS 1981) and by others (Thomson 1979; Tracy and Noll 1979; Hodgson et al. 1981) who have considered using solid state devices operating as multi-spectral push-broom cameras, is the difficulty in calibrating such large numbers of individual detectors.

The problem is mostly a conceptual one, since the increasing number of calculations involved are easily handled by increasingly powerful computers. As will be discussed below, calibration of the half million detectors in the FLI has presented problems, many of which have been related to the very small size of the PDP 11/04 calibration computer with which the FLI was delivered. Significant improvements are possible using the PDP 11/34 based IOS image processor to perform the calibrations with floating point arithmetic and image processing routines not available to the smaller machine. However, even using the larger PDP 11/34 computer, processing the large amounts of data produced by the FLI is slow and time consuming. As a result only a very small amount of the June and December data has been fully analysed. Access to an even larger and faster computer would speed up analysis considerably. It will become mandatory if FLI data is ever to be produced for many users in an operational mode.

## 2. EVALUATION OF THE FLUORESCENCE LINE IMAGER INSTRUMENT PERFORMANCE

### 2.1 Optical Response

The net apparent responsivity of the five FLI camera modules has been calculated using the January 1985 calibration data and assuming linearity of response. Expressed as digital counts output per unit power incident illumination, these are five two dimensional  $288 \times 385$  element matrices. They will be a product of the transmission of the lenses and reflection grating inside each camera, the spectral response of the individual CCD's and the charge transfer efficiencies. The general shape of the matrix for camera 3 is illustrated in Fig. 2, in which the responsivity of each element in the array for an integration time of 300 ms is represented as a colour level in a digital image.

Plots across the responsivity matrices (Fig. 3 and 4) summarize the response in the spectral and spatial dimensions for each camera and show some details of the structure of the arrays. With the exception of camera 4, all are similar, with differences in their responsivities amounting to about 5% near the centre of the spectrum and increasing to about 15% at the blue end. Camera 4 is about twice as sensitive at shorter wavelengths than the other four. Except for camera 4, the spectral shape of the responsivities of all five cameras are similar to that given as typical for P8600 EEV arrays by the manufacturer (EEV 1982). The decrease in spectral responsivity at wavelengths longer than 700 nm is due to the blazing of the diffraction grating in the FLI cameras. The responsivities shown in Fig. 3 are expressed per pixel and per 300 ms integration time. They will be increased significantly by band forming and longer integration.

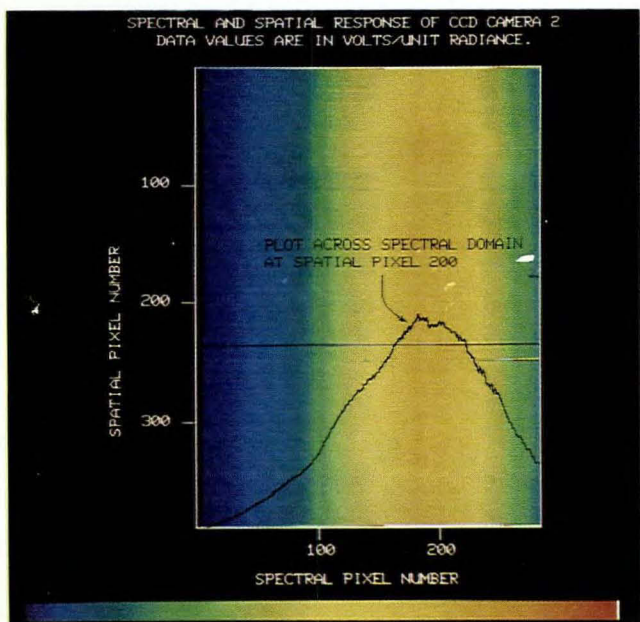


FIG. 2. The relative shape of the responsivity matrix for camera 2. The magnitude of the response (counts / Watt  $\text{cm}^{-2} \text{sr}^{-1} \text{nm}^{-1}$ ) for each element is indicated by the colour scale which represents relative values between 1 (blue) and 255 (white).

All five cameras exhibit very similar response across their spatial dimension (Fig. 4), with a banding presumably reflecting the method of their manufacture. Severe blemishes can be seen where this plot intersects such features; at spatial pixel 236 on camera 2, 127-128 on camera 3, 123-125 on camera 4, and 356 on camera 5. The first two and last two rows of spatial pixels on all arrays have anomalously high gains.

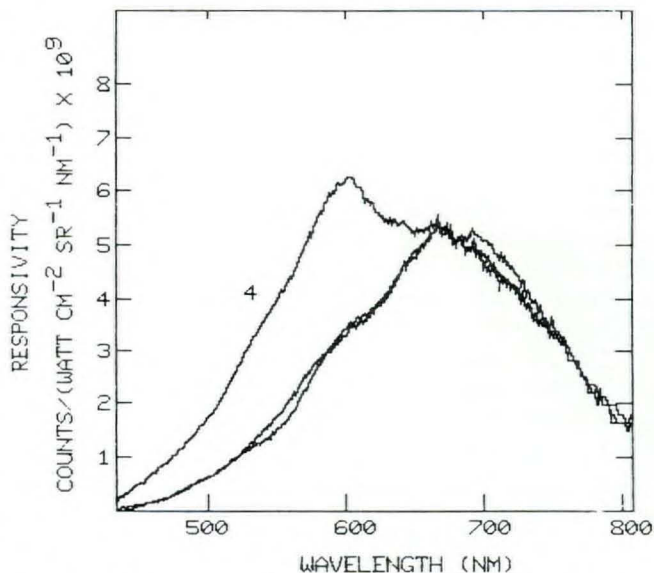


FIG. 3. Plots of the spectral variation of responsivity of cameras 2 to 5 at spatial pixel 100, expressed per pixel and for an integration time of 300 ms.

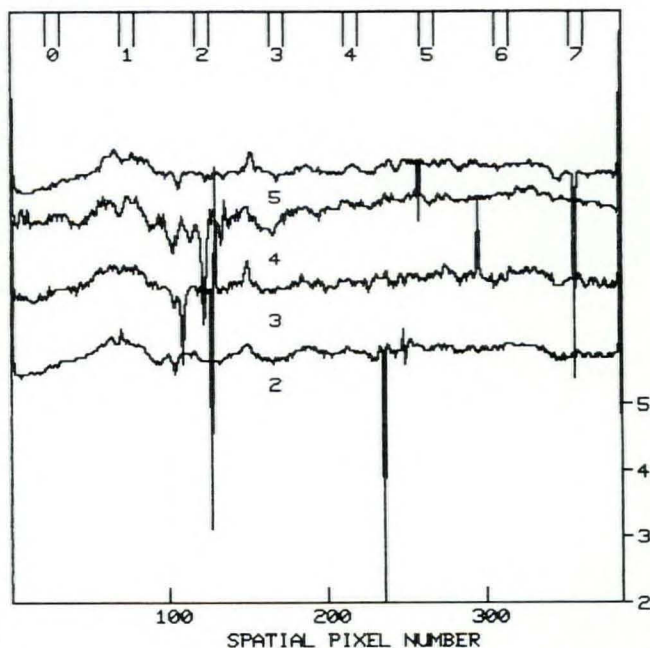


FIG. 4. Plots of the variation of responsivity across the spatial dimension of cameras 2 to 5 at spectral pixel 200. Bars at the top of the plot indicate spectral mode band placements for the December 1984 mission. Spikes on the traces represent blemishes on the arrays.

TABLE 3. FLI system responsivity counts/(W·cm<sup>-2</sup>·sr<sup>-1</sup>·nm<sup>-1</sup>) × 10<sup>10</sup> in spatial mode, averaged for entire bands and a 300 ms integration time.

Camera #	spectral band number							
	0	1	2	3	4	5	6	7
	(number of diodes in spectral band)							
	(8)	(8)	(8)	(9)	(11)	(11)	(5)	(10)
	approximate wavelength limits of each band (nm)							
	467-476	541-550	586-596	633-644	659-673	673-687	708-713	746-759
1	camera 1 not operating at the time of the January calibration							
2	0.27	1.24	2.61	3.98	6.13	5.98	2.51	3.99
3	0.30	1.24	2.60	3.97	6.11	5.96	2.40	3.98
4	0.90	3.47	5.27	5.44	6.72	6.41	2.60	3.98
5	0.26	1.38	2.55	4.13	5.89	5.69	2.30	3.75

Table 3 lists the responsivities for the eight spectral bands in the spatial mode (December 1984 definition) of cameras 2 to 5 calculated from the January 1985 calibration data, which was obtained at a 300 ms integration time. Values are averages for each band, that is, they do not reflect the variability across the spatial dimension of the arrays.

These responsivity factors are in effect the gain calibration of the instrument, and assume that the gain of all diodes in all arrays is linear with input. The instrument output in the absence of input signal (the dark signal) is treated as a fixed offset and is normally removed in real-time.

The minimum light level at which the FLI gives a useful output will depend on the responsivity (and therefore the spectral band), the number of pixels summed to make the band, the integration time and the noise level. A complete analysis of noise properties for all parts of all five arrays has not yet been completed. However, analysis of laboratory data discussed later has shown that readout noise (as standard deviation) is equivalent to about 2.5 counts per pixel in the

vicinity of band 4 in camera 3. The Noise Equivalent Radiance for this readout noise floor will be  $4.1 \times 10^{-11}$  Watts cm<sup>-2</sup> sr<sup>-1</sup> nm<sup>-1</sup>.

## 2.2. Noise Performance

### 2.2.1. Fixed Pattern Noise

With the shutters closed, the output from each FLI array has a fixed pattern similar to that shown in Fig. 5. There will be a constant offset due to the input setting of the analog to digital converter, to which is added the dark current signals which differ for each diode on each array. Random noise is also superimposed onto this pattern.

As shown in Fig. 5 and 6, diodes having a spatial coordinate above about 240 have from 3 to 25% higher output

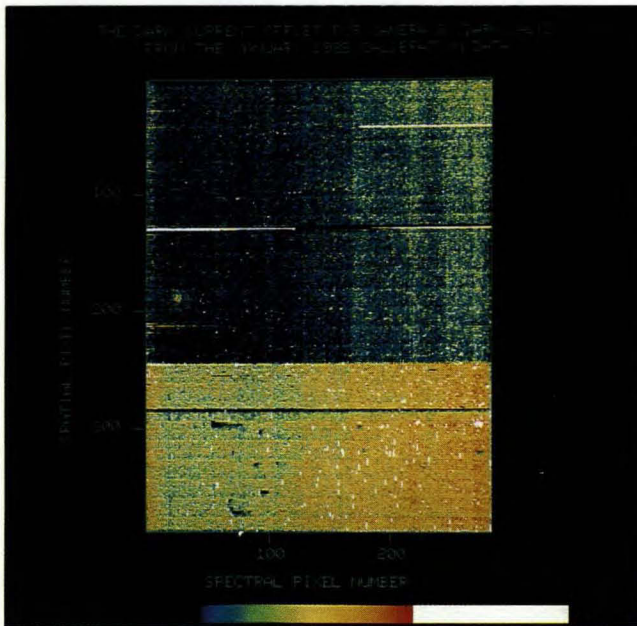


FIG. 5. The two-dimensional structure of the dark current offset (DARK.CAL;3) for camera 3 from the January 1985 calibration.

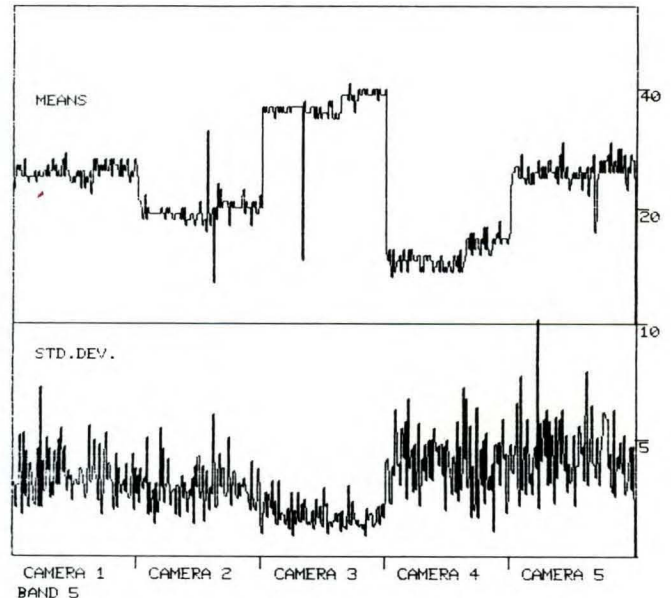


FIG. 6. Variations of the mean dark current offset and standard deviation for 11 scanlines of dark data for every 4th spatial pixel in band 5, June 21 1984. Shutter closed, real-time dark and uniformity corrections disabled, integration time 400 ms. Linear current controllers operating.



than those below 240. This "offset step" is greatest for camera 4 and least for camera 5. There is some indication that this step may be introduced in the analog signal chain.

Figure 6 also shows the noise level (expressed as standard deviation per pixel) across the array, which during the June test flights was greatest in cameras 4 and 5.

The fixed pattern dark offset is small relative to the full well signal (from 2 to 10 counts per 100 ms, depending on the camera). The dark signal contribution is temperature dependent (EEV 1982), but during operation of the FLI the dark current levels are designed to be controlled through temperature stabilization of each array. The roughly fixed levels are removed in real-time during flight.

Figure 7 compares the dark current offsets for dark data obtained during the June 1984 flights with the shutters closed and DARK.CAL data from the January 1985 calibration. The aircraft data are for spatial mode band 5 (June 1984 definition: spectral diodes 184-192), while the DARK.CAL data were subsampled and averaged to form the same band. The aircraft data are a time average of 11 scans at 400 ms. However, the laboratory data are the average of 16 frames at 300 ms and therefore represent 10% longer integration. These plots suggest that the shape of the dark current offset for camera 2 has changed. The increase in dark signal seen on cameras 1 to 4 above spatial pixels 260 in June (Fig. 6), can be seen in DARK.CAL;3, and 4 but it is not present in DARK.CAL;2.

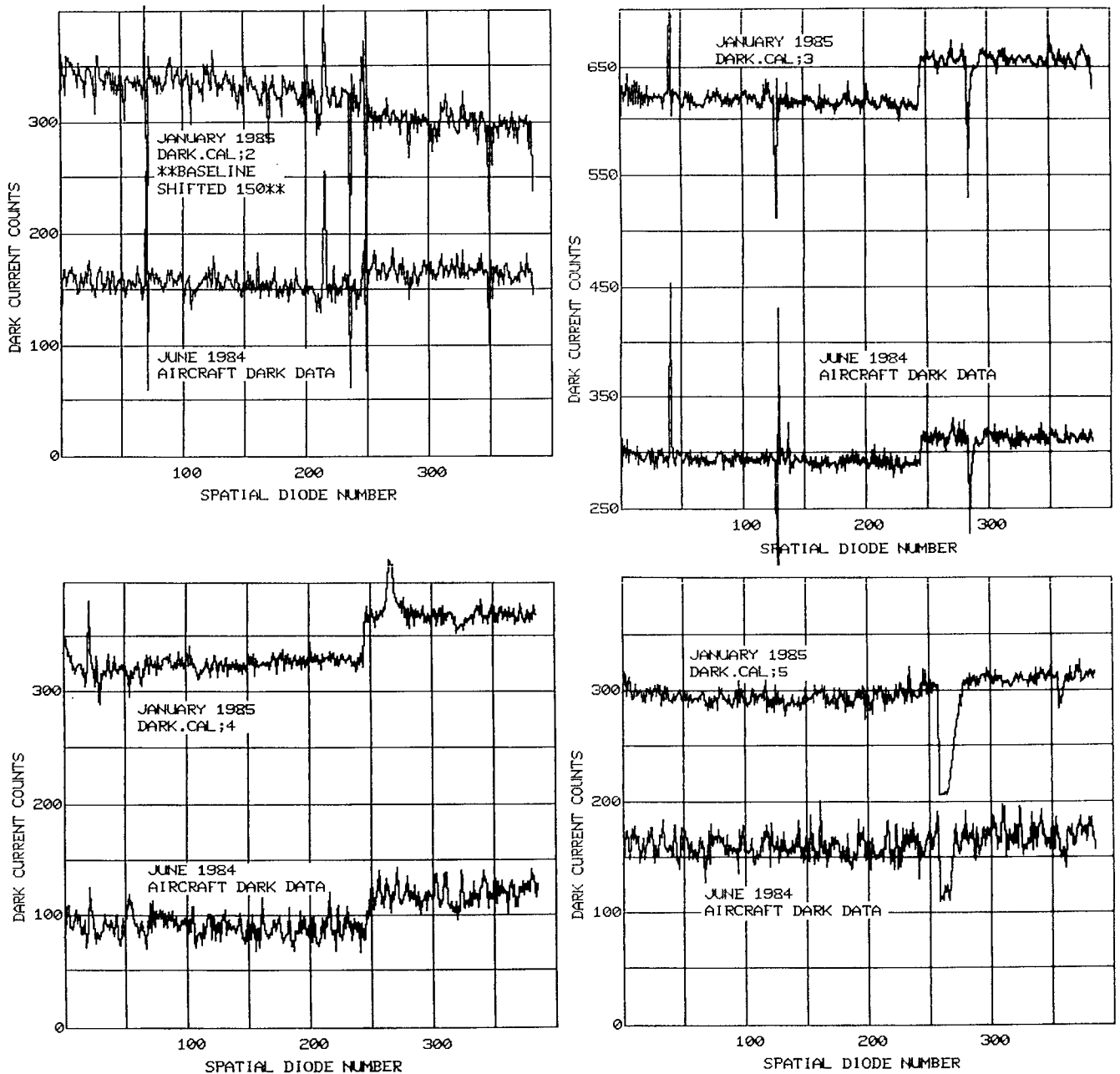


FIG. 7. Comparison of the dark current offset for a spatial band (spectral diodes 185-192) in flight data obtained with the shutters closed and in laboratory DARK.CAL data. Aircraft data are the average of 11 scans at 400 ms integration. Lab data are for 16 frames at 300 ms. Note the baseline change for camera 2 and scale change for camera 3.

Except for differences in noise levels, which represent engineering improvements between June and December and possibly the difference between lab and aircraft environments, cameras 3, 4, and 5 show similar structure in both measurements. The peak near spatial diode 265 in DARK.CAL;4 is part of a band of high signal across the spectral dimension of the array. This is due to an incomplete shutter closure, which has been occasionally noted in lab data.

A second type of fixed pattern noise was observed in image data from bands with low signal amplitude (bands 0 and 7 over water) in early FLI data and in the June test data. A "herring-bone" pattern was being caused by electronic pick-up in the instrument. The switching current controllers were thought to be causing this problem, particularly those which were originally installed in the FLI to control the cooling of the instrument through a feedback loop. Accordingly, a second set of linear analog controllers was installed and tested on the June flights. There was a dramatic reduction in the amplitude of the herring-bone noise in band 7 of camera 4 and a lesser reduction in camera 5, but cameras 1 and 3 were still affected.

Itres and Moniteq investigated the noise problems in more detail in the laboratory during October and November of 1984 and were able to show that the major sources of system noise until then had been the switching mode power supplies which were originally used at several locations within the system (Itres 1984). Consequently all power supplies were replaced with the analog versions for the December flights over Chesapeake Bay. Some herring bone pattern can still be detected in the December spatial imagery, however, and the flight data of Fig. 8 show the effect of an additional contribution to the system noise (see below).

### 2.2.2. Random Noise

The random noise level of the signals read out from the CCDs will consist of two components, shot noise and read-out noise. The statistical nature of the accumulation of electrons in each CCD sensing element (diode) leads to a fundamental variance in this number, i.e. "shot noise", whose value is numerically equal to the number of electrons. In addition, read-out noise is added by the electronics used to read-out the low level signals from the CCDs. These signals are vulnerable to the pick-up of radiated or conducted noise, which may have a regular character, but which will add a random contribution to the effective read-out noise.

The analog to digital converters have also been found to have a slightly anomalous response at certain signal levels. This will add a small, variable contribution to the read-out noise. These converters will be replaced when improved versions are available from the manufacturers.

Since variances of normally distributed random signals add, we may write:

$$V_e = n * s_e + (n * r_e) = S_e + (n * r_e)$$

for the total variance when a band is formed by adding  $n$  roughly equal element outputs,  $s_e$ , together to form the total output  $S_e$ . (Readout noise variance,  $r_e$ , is added as each

element of the band is read out.) All levels are expressed in terms of the equivalent number of electron charges, and the variances have units of electron charges squared.

If the analog to digital converter gain is set so that 1 analog to digital unit (ADU) is equivalent to  $K$  electrons, then in ADUs:

$$V = V_e / K^2, S = S_e / K, r = r_e / K^2$$

$$\text{Hence: } V = S / K + (n * r)$$

$S$  is now the mean value of the signal that is recorded on tape (in ADUs), and  $V$  is its predicted variance if  $K$  and  $r_e$  are known.

Figure 8 shows laboratory measurements of how the observed variance,  $V$ , varies with  $S$  for different values of  $n$ , the number of elements (i.e. pixels or diodes). These curves can be reasonably well fitted by:

$$V = 0.018 * S + 5.5 * n$$

implying  $K = 1 / 0.018 = 55$  electron per ADU, and  $r = 5.5$  ADUs.

This implies that signal saturation (4095 ADUs) is achieved by a given element when 225,000 electrons have been collected. This is comfortably within the specified 300,000 "full well" capacity of each site, without sacrificing too much sensitivity by setting this value too low.

Noise is usually expressed as the square root of the variance, or standard deviation, which then gives a dimensionless signal to noise ratio ( $S/N$ ) when divided into the signal level. The maximum of this ratio occurs when the FLI is adding 16 near saturation signals (4095 ADUs) from 16 elements to form a total band signal of 65520. The variance is then:

$$0.018 * 65520 + 5.5 * 16 = 1270$$

giving a standard deviation of 36, and a signal to noise ratio of 1840. This agrees with an analysis by Itres Ltd. in November 1984, who also confirmed our observation that the noise on the June dark data varied between cameras (Itres 1984). As

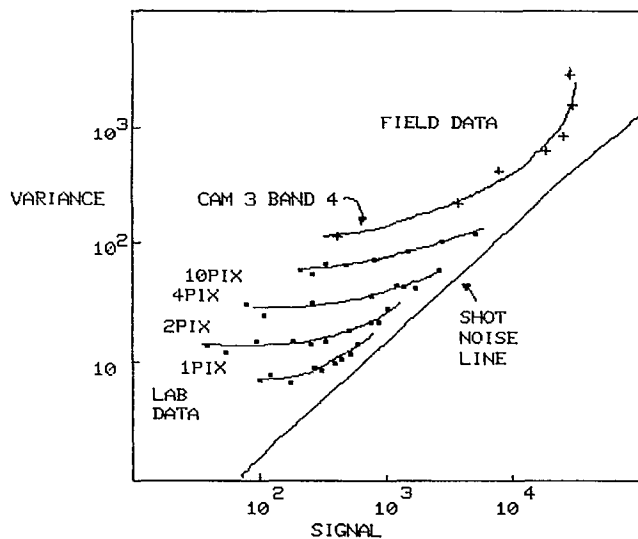


FIG. 8. An analysis of signal-to-noise properties of the FLI from data collected in the lab by Moniteq Ltd, and in the field during this project. Variance at signals below about 300 is governed by read-out noise. Shot noise raises the noise levels above this.

pointed out in the CCUSS report, the best operation will be near full-well capacity on the arrays.

The observed standard deviation of the read-out noise is 2.3 ADUs, or 130 electrons, slightly more than the 100 electrons specified for the EEV P8600 arrays.

Figure 8 also shows signal variances derived from image data recorded in flight. These were calculated from uniform areas of a scene so that natural signal variance is minimized. These higher variance values are confirmed by analysis of dark data recorded in flight. The aircraft environment therefore appears to cause extra noise pick-up, and some of the observed read-out noise in the laboratory may also be due to this.

Further work is planned to try to reduce the pick-up contribution to read-out noise. The shot noise is the dominant factor for high signal levels, but the above equations show that at signal levels below about 1/13 of saturation the read-out noise will dominate. This is especially important at blue wavelengths where the CCD sensitivity is low, and signal levels are therefore always small.

### 2.2.3. Other Effects

Apart from the random and fixed pattern digital noise on the output of all arrays, the June and December flight data were both affected by intermittent bad scanlines. Data from each band of the FLI is recorded on separate tracks of the Bell and Howell HDDT, and later stripped in the laboratory and formatted onto computer compatible tapes (CCTs). Both the recording and the stripping process require careful set-up of the HDDT.

Bad scanlines occur with variable frequency in the CCTs of FLI data. These include dropouts or lines which are entirely zeros and loss and reacquisition of data synchronization on the High Density Digital Tape (HDDT) part way across the scan.

This problem was severe on some of the early flights, however, modifications to the HDDT interface by CCRS during July and August 1984 have since improved recording fidelity.

## 2.3. CCD Array Non-Uniformities

### 2.3.1. Linear Effects

The responsivity of CCDs is in general very nearly linear (Thompson 1979; Wharton et al. 1981; EEV 1982), but variation of response across the sensor area must be anticipated, due to material heterogeneities and small variations in the size of each sensor element. These variations are removed in the FLI data calibration procedure.

The non-uniformities present in the EEV P8600 CCD arrays used in the FLI have been investigated using the data from the March 1984 calibration exercises carried out by Moniteq Ltd. Figures 8 to 10 illustrate several types. Linear variations in the response which can be successfully removed in calibration include:

1) Regular spatial banding — All five arrays have a similar banding pattern in the spatial dimension resulting

from differing gains (Fig. 4 and 9). Spatial pixels 1,2,384 and 385 have very much higher gain than their neighbouring pixels in all cameras.

2) Irregularities — In addition to the non-uniformities noted above which appear on all arrays, array number 1 shows what appears to be a scratch or drop of glue between spatial pixel number 180 and 240, in the vicinity of spectral pixel

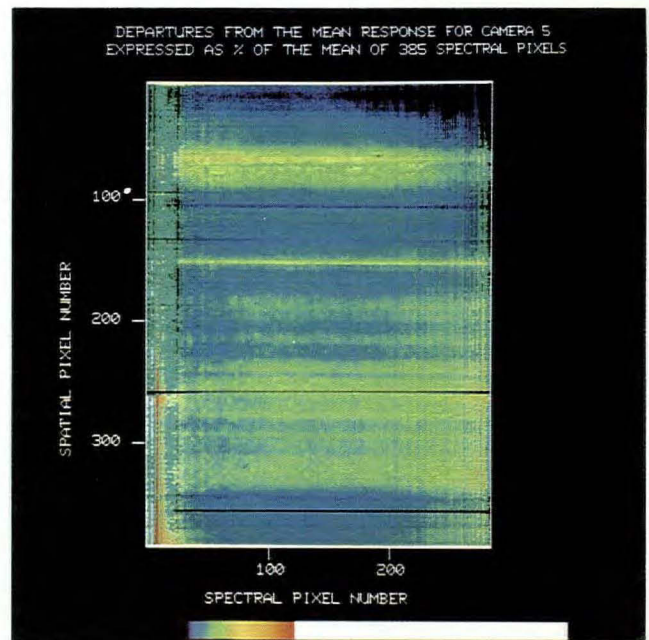


FIG. 9. Departures from the mean response on camera 5, expressed as a percentage of the mean for each column of spectral pixels. Minimum (blue) is approximately 89% of the mean, maximum sensitivity is near 110%. The apparent banding is presumably a function of the manufacturing process.

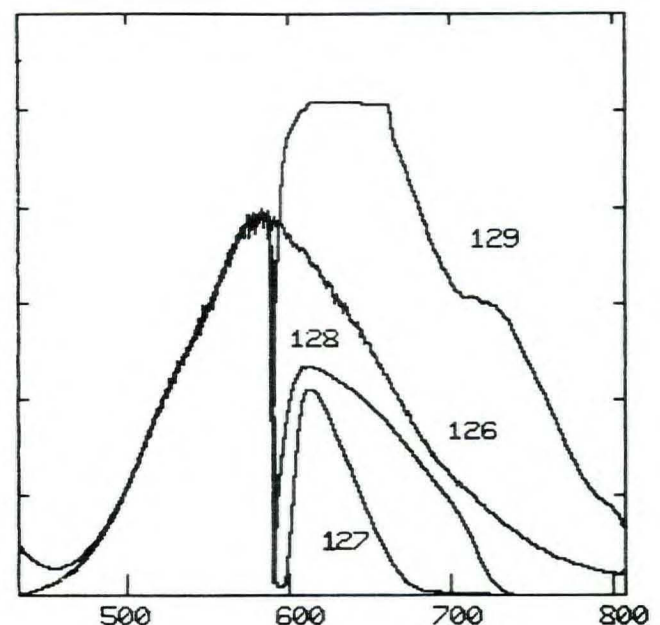


FIG. 10. Plots across the spectral dimension of the TRUE.CAL from camera 3 (January 1985 data), showing an example of a blemish on the array from that camera.

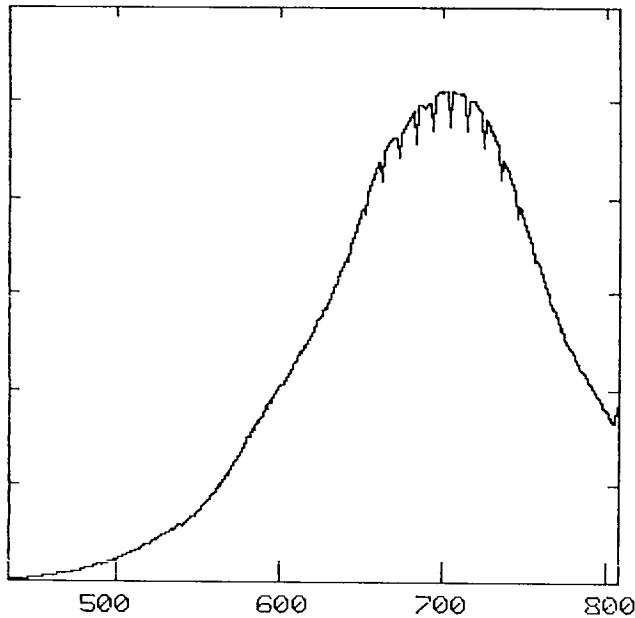


FIG. 11. Plot across the spectral dimension of TRUE.CAL;2 (March 1984 data) at spatial pixel 58 to show the grid pattern of low gain pixels in this part of arrays 1 and 2.

number 230 – 240. Array 4 has a large “shadow” across the centre of the spectral dimension above spatial pixel number 200.

### 2.3.2. Non-Linear Effects

Variations of the CCD response which are non-linear will not be removed by the present one-point gain calibration. While small non-linearities in average detector responses do not appear to be affecting the data, occasional major “blemishes” do appear in the calibrated image and spectral data. Two effects which have been noted are:

1) “Hot” or “cold” pixels — Pixels with very different gains from their neighbours appear throughout each of the arrays. Generally, these occur as bad “rows” of pixels across the spectral dimension of the array. For instance, Fig. 10, which shows cuts across the spectral dimension of the March 1984 TRUE.CAL calibration data for camera 3, illustrates a group of bad rows in the vicinity of spatial pixel 126.

2) Grid pattern in the response of cameras 1 and 2 — The March 1984 TRUE.CAL calibration files for cameras 1 and 2 showed a regular grid pattern of high and low gains across the first 65 spatial pixels and the PCF.CAL (Pixel Correction Factors) and BCF.CAL (Band Correction Factors) calibration files calculated for these cameras also reflected this variability. However, since the pattern repeated itself in uniformity corrected data, the calibration was suspect. The January 1985 calibration SGN.CAL;2 file also shows this structure but with less amplitude and at a different spectral position on the array because of the bluer peak radiance used in that calibration. It is only visible where signal levels are greater than about 48,000. This phenomenon has not yet been fully investigated and its cause is unknown.

## 2.4. Spatial and Spectral Resolution

### 2.4.1. Spatial Resolution

The spatial resolution of the FLI is determined by the camera optics, and the size and horizontal spacing of the array elements. It will change with the wavelength of the light falling on the array. In the horizontal direction, (spatial dimension in the FLI) the theoretical modulation transfer function (MTF) of EEV P8600 arrays at the spatial Nyquist frequency (i.e. at the limit of spatial resolution) is about 64% at wavelengths shorter than 700 nm but decreases to 46% at 800nm (EEV 1982). This will lead to a slight decrease in resolution at longer wavelengths.

We do not have enough laboratory data to calculate the full spatial resolution or Modulation Transfer Function for the FLI system. However, there is some laboratory data from the September 1983 camera alignment exercise (Moniteq 1983) which shows plots of the response of each camera to a scan of a collimated light source for a spectral band centered at 648 nm. The data indicate the angular resolutions along the flight direction to be 0.96, 0.90, and 0.86 mrad for cameras 1, 2, and 4, respectively (full width to half maximum). These values compare well with the nominal value defined by the entrance slit, which is 1.5 pixels or 0.95 mrad wide. In practice, this resolution is dominated by motion blur for flights at all but the highest altitude.

For the cross track direction, data is more limited. The angular resolution is about 0.83 mrad at the centre of camera 3. This is larger than the angular size of a single CCD pixel (0.635 mrad) due to a combination of optical blur and detector MTF.

### 2.4.2. Spectral Resolution and Accuracy

The spectral dispersion of the FLI cameras has been measured in the laboratory (Gower 1983; Moniteq 1983) by observing the spectral widths and positions of lines from a Hg-Argon lamp. The results show a spectral resolution of 2.5 nm, and a wavelength interval of about 1.3 nm between diode centres.

After alignment with the 632.8 nm line of a He-Ne laser, these measurements show less than 0.4 pixel variation across the spectral dimension of all five cameras. The observation that the group of Oxygen absorption bands between 760 and 762 nm appears in the data as a minimum at 762 nm confirms the alignment.

### 2.4.3. Spatial Alignment of the FLI Camera Modules

Since the camera modules must be periodically removed from their mounting in the FLI for calibration and maintenance, they are not mounted permanently and they

must be re-aligned after each removal. This procedure was carried out in September 1983 using the CCRS Precision Motion Simulator and a collimated light source, and involved a yaw, pitch and roll alignment of each camera relative to camera 3. Data from the tests themselves indicated that the centres of the cameras were aligned to within 0.29 mrad rms, with a variation of 0.89 mrad across the cameras.

While it is not possible to accurately estimate the misalignments from field data, roll and pitch differences can be detected as departures from the original 8 pixel overlap between cameras and as discontinuities in spatial features which cross camera boundaries. Yaw alignment can be very roughly checked in images of linear features which cross the field of view of all five cameras (such as the Chesapeake Bay bridge-tunnel in the December flight data).

On the June 1984 flights the FLI produced spatial imagery in which cameras 1 through 4 were aligned, but camera 5 was pitched 2 pixels (1.6 mrad) ahead of the others. No re-alignment was done after maintenance operations during the summer and data collected on the December flights showed evidence of considerable misalignment. Relative to camera 3, camera 2 was pitched ahead by 2 pixels (1.6 mrad) and rolled towards nadir by about 8 diodes. Camera 4 was pitched ahead by 3 or 4 and camera 5 was pitched back by 1 or 2. The yaw appears to be correct.

The current alignment (July 1985) is sufficiently improved that the rms pitch errors are reduced to 0.082 mrad (0.13 pixels) for the four cameras that were in operation at that time. Yaw errors have not been analysed but are expected to be similar. Roll (overlap) has been adjusted to within 0.13 mrad (0.20 pixels) rms.

## 2.5. Camera Focus

In data from their Panama City flights, Moniteq found that imagery of roadways in camera 2 was blurred in the along-track direction. They felt that the yaw adjustment plate for this camera had "become springy" and was allowing vibration. In order to prevent this vibration, they remounted camera 2 on special washers to stiffen the mount prior to the December exercise.

This modification appears to have solved the problem, since along-track smearing was not evident in land imagery acquired in December.

## 2.6. Optical "Ghosting"

Spurious optical ghost images caused by reflection from the front surface of the grating were observed in image data from the December 1983 and June 1984 flights. The magnitude of the ghost image amounted to about 10 to 15% and varied between cameras. Subsequently, an attempt was made to alleviate the problem by inserting a mask on the plano-convex lens and tilting the grating in each camera. After the modifications, ghost images could not be seen in the Ottawa River test flight or in the Panama City data (Moniteq 1985). However a careful examination of band 7 spatial imagery obtained December 13, 1984 over the bridge-tunnel at the mouth of Chesapeake Bay, shows a small (~1%) ghost in camera 2 still exists. We have not yet been able to check the other cameras, since this requires a bright object at one edge of the camera and very dark and uniform water at the other.

### 3. CALIBRATION OF FLUORESCENCE LINE IMAGER DATA

#### 3.1. Calibration of the FLI Arrays

To obtain an absolute calibration in radiance units for FLI image data, a conversion factor is needed:

$$\text{Radiance}_{ij} = \frac{\text{counts}_{ij}}{R_{ij}}$$

Where  $R_{ij}$  is a measure of the responsivity of the single detector  $i,j$  in a single camera.  $R_{ij}$  is measured in the calibration procedure by recording the dark-corrected camera response (TRUE.CAL<sub>*ij*</sub>) to nearly uniform illumination in an integrating calibration sphere. The uniformity of the sphere is specified by RISPL<sub>*i*</sub> and the spectral nature of the illumination by RISPC<sub>*j*</sub>.

$$R_{ij} = \frac{\text{TRUE.CAL}_{ij}}{\text{RISPL}_i \times \text{RISPC}_j \times 12.68 \times 10^{-7}} = \frac{K}{\text{PCF.CAL}_{ij}}$$

The units of  $R_{ij}$  are counts / Watts cm<sup>-2</sup>sr<sup>-1</sup>nm<sup>-1</sup>. In the above, PCF.CAL<sub>*ij*</sub> contains the calibration information for all detectors in a single array. There are 5 PCF.CAL's and 5  $K$ 's corresponding to the five cameras. For each camera, the constant  $K$  is used to scale the values for processing and storing within a 16 bit range. Its value is set in practice by choosing a Scale factor  $S$  during calibration ( $S$  is currently 150). The resulting value of  $K$  can be found from the data at any element of the  $i,j$  matrix. Using the element where RISPC<sub>*j*</sub> × RISPL<sub>*i*</sub> is equal to 1, which for the January 1984 calibration is known to have represented a lamp power of 12.68 Watts cm<sup>-2</sup>sr<sup>-1</sup>nm<sup>-1</sup>:

$$K = \frac{\text{PCF.CAL}_{ij} \times \text{TRUE.CAL}_{ij} (\text{counts}^2)}{12.68 \times 10^{-7} (\text{Watts cm}^{-2}\text{sr}^{-1}\text{nm}^{-1})}$$

$$\text{For camera 2, } K = \frac{3165 \times 1552}{12.68 \times 10^{-7}} = 3.874 \times 10^{12}$$

The responsivity for element  $i,j$  ( $R_{ij}$ ) will not be the same as  $R'_{ij}$  if different bands and integration times are used in the calibration and in the field observations. Then:

$$R_{ij} = R'_{ij} \times \frac{\text{integration time}_{\text{obs}}}{\text{integration time}_{\text{cal}}} \times \frac{\#\text{diodes in band}_{\text{obs}}}{\#\text{diodes in band}_{\text{cal}}}$$

Laboratory exercises to collect amplitude and spectral calibration data have been carried out by Moniteq in March 1984 and January 1985, using the facilities at CCRS. This involves recording the output of each FLI camera while it is viewing a uniform light source (a 30 cm calibration sphere illuminated with two 10-W Osram tungsten halogen lamps). The spectral and spatial radiance character of the calibration sphere was measured against a secondary standard (a Photo-Research Ltd. Spectraspot) which had been calibrated against a National Research Council calibration lamp and barium sulphate panel (Moniteq 1984a). Since only one calibration sphere exists, each camera module must be calibrated separately. The FLI output is recorded on 8" diskettes, which can

then be used as input to calibration routines written by Itres Ltd., Calgary. These calibration procedures calculate a uniformity correction for each array which is stored in an EPROM for real-time calibration if desired. The potential advantage of real-time calibration is a very significant reduction in data processing.

Due to memory and disk space limitations within the calibration computer (a PDP 11/04), the Itres calibration process requires sequential execution of several separate programs. Each program produces intermediate disk files which are then used by the next program in the sequence. The final result of the calibration process is an array of integer uniformity correction coefficients which, when multiplied by the FLI band diode values, correct for relative gain differences between elements on the CCD arrays.

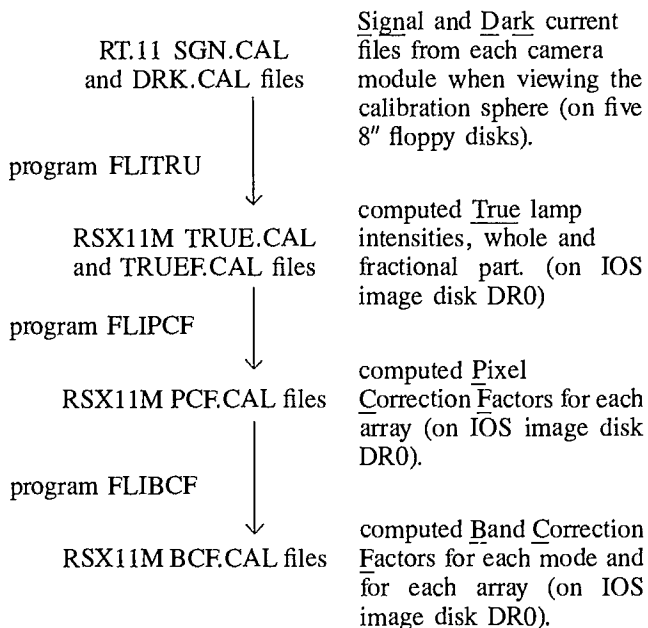
As will be discussed in section 4.1.1 to follow, the precision of the radiometric calibration is greatest between 600 and 700 nm, and is reduced at wavelengths less than 500 nm because of the low sensitivity at these wavelengths and the lack of blue light in the calibration lamp. All arithmetic operations in the calibration sequence are presently performed using 16 bit integer arithmetic and require scaling factors to maintain precision throughout the operation. However the final step in the calibration, multiplication of the raw input signal counts by the Band Correction Factors (BCF) causes a significant loss in arithmetic precision because the BCFs are fractions less than one. This is necessary because of the need to avoid integer overflow, but the result is that the arithmetic precision of the calibrated data is reduced to nearly 9 bits above about 590 nm. This could be avoided by using floating-point arithmetic instead of integer, however this would require use of a larger computer than the present calibration computer.

The calculation of the uniformity correction and burning of the EPROM is intended to take place before the instrument is flown, so that real-time corrections can be made. In fact very little real-time uniformity corrected data was obtained on the June flights and none on the December flights. We have not yet analysed uniformity corrected data and have concentrated on the investigation of the calibration itself. Since the real-time corrections would greatly reduce the data processing burden, there is a significant advantage to using them. This will become practical when a good quality calibration is obtained.

#### 3.2. The IOS Calibration Routines

Calibration software written for the IOS Image Processing System provides an alternative method of calibrating the FLI and applying uniformity corrections to uncalibrated FLI data. As of May 1985, the IOS uniformity correction procedure was identical to the Itres procedures in order that step

by step evaluation and comparisons could be made. The following flowchart summarizes the procedure:



The output BCF.CAL files are then used to calibrate FLI field image data in any one of the three modes. The IOS procedure can also use TRUE.CAL and TRUEF.CAL files supplied on diskette generated by the Itres routine as carried out using the FLI calibration computer.

A separate BCF.CAL file must be calculated for each FLI operating mode and whenever the spectral or spatial band definitions are changed. It is these BCF.CAL values which are used by other programs to correct individual pixels within bands for gain variations with respect to other pixels. Since all of our work on this project to this point has involved analysis of image data on the video display system, we have utilized uniformity corrected image data only, i.e. data with a relative calibration using scaling factors designed to maintain as much precision as possible.

This relative uniformity calibration was replaced by a true radiance calibration using floating point arithmetic in July 1985.

## 4. EVALUATION OF THE CALIBRATION OF THE FLUORESCENCE LINE IMAGER

### 4.1. Radiance Calibration

#### 4.1.1. Spectral Radiance Calibration

The EEV CCD arrays are known to have low responsivity at blue wavelengths (EEV 1982). However, in calibration this is further aggravated by the fact that the calibration lamps used to calibrate the FLI camera modules are very red. In order to avoid saturating the arrays at longer wavelengths, integration times must be used which allow very little blue signal to be captured.

This problem was severe in the March 1984 calibration. The signal levels at short wavelengths were at or below the noise levels at the time and the effect of the lack of blue light in the March 1984 calibration can be seen in field data uniformity corrected with this data (Fig. 12). Difference spectra from two different altitudes should show a lambda to the fourth shape ( $\times$  sun radiance spectrum) because of Rayleigh scattering (sun spectrum from Kondrat'ev (1973) for 3000m altitude). The fact that the difference calculated for spectral data obtained in June, 1984 over Lake Ontario begins to fall off around 520 nm is evidence that the SGN.CAL from the March 1984 calibration was too large at the blue end, either due to an underestimate of the dark or an overestimate of the signal. The dark levels were nearly equal to the signal levels on this part of the array.

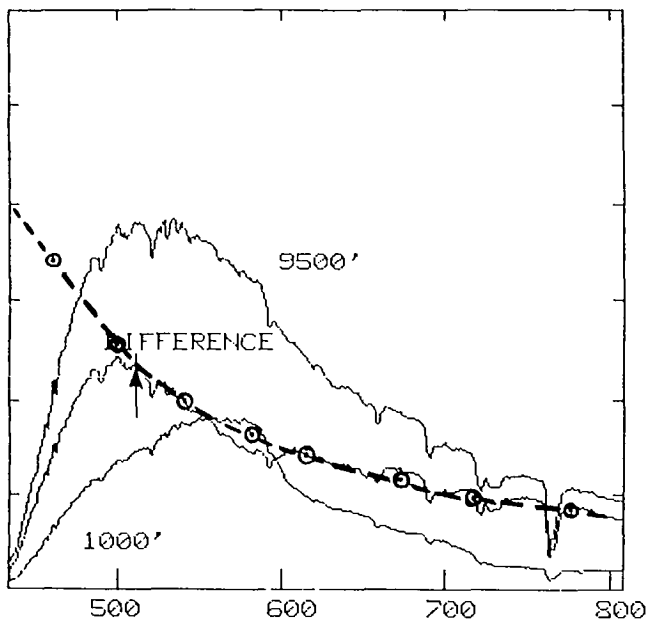


FIG. 12. Upwelling spectra (calibrated with the March 1984 calibration data) from the same location in Lake Ontario, but from different altitudes. The difference should represent scattered light and absorption in the intervening atmosphere, and should follow a  $(\text{wavelength})^{-4}$  law. The departure from the expected curve (Rayleigh scattering  $\times$  sun's spectrum) indicates that the March 1984 calibration is incorrect below about 510 nm.

In an attempt to rectify this problem, the relative amount of blue light in the January 1985 calibration was increased. Blue BG23 colour glass filters were used to reduce the amount of longer wavelength light in the calibration sphere and integration times were increased (Moniteq 1985). The effect of this has been to improve the spectral calibration between 480 and 520 nm because of a more accurate estimate of the low blue output, and can be seen in Fig. 13. The difference spectrum now follows the expected Rayleigh curve ( $\times$  sun radiance spectrum) to 480 nm. The departure from the expected Rayleigh curve below 480 nm must mean that the PCF.CAL is still too small however. The SGN.CAL therefore must still be too large, suggesting a negative dark drift or, more probably, a scattered light contribution.

Below about 445 nm (this limit varies for each camera) the uniformity corrected upwelling spectra drop to zero. This is caused by the fact that the absolute values of the TRUE.CALs were low enough to cause the PCF.CAL to be larger than 65,536. We have therefore arbitrarily set the PCF.CALs to zero to indicate that this data cannot be calibrated. This problem is solved by using floating point arithmetic in place of the integer calculations.

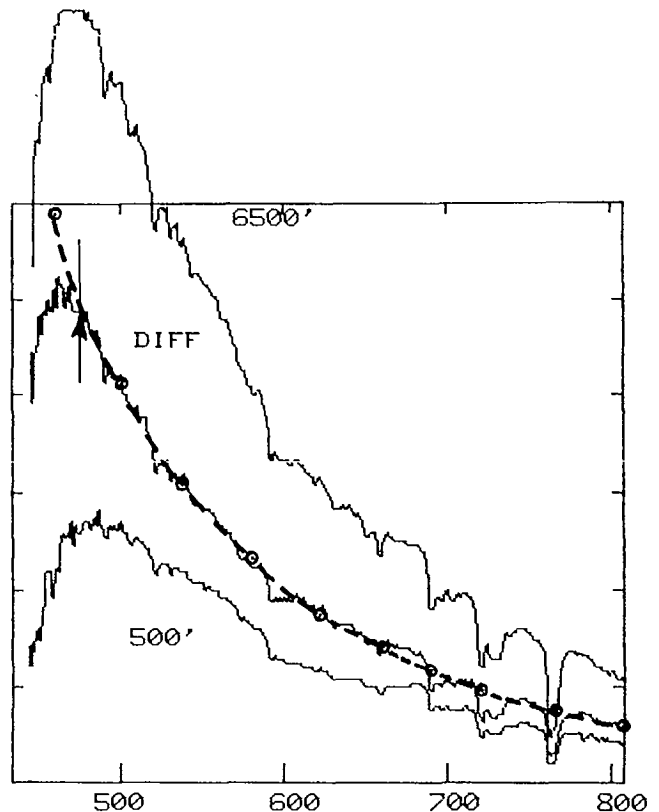


FIG. 13. Upwelling spectra (calibrated with the January 1985 calibration data) from the same location off the coast of Virginia, December 15, 1984. The departure of the difference from the expected curve (Rayleigh scattering  $\times$  sun's spectrum) is now improved down to about 480 nm.



#### 4.1.2. Inter-Camera Errors

The requirement that the five camera modules be separately calibrated leads to the possibility of differences in calibrations among them if, for instance, the output of the calibration lamp changes during the course of the exercise or the calibration sphere cannot be reproducibly mounted on the cameras. Spatial image data uniformly corrected with the March 1984 calibration data showed gross amplitude differences which could only be a result of incorrect calibrations. We accordingly inserted a camera gain adjustment factor into the calibration procedure at IOS. These gain adjustments were empirically calculated from spatial image data with camera 3 as reference. Table 4 summarizes the gain adjustments required to remove these amplitude differences in the June flight data.

For the January 1985 calibration exercise, special precautions were taken to regulate the current supply to the lamps. The stability of the sphere as indicated by the photodiode was estimated to be 0.3% over several hours of operation (Moniteq 1985). This was expected to solve the problem. However, as shown in Fig. 14, the amplitude variations are still present for December 1984 spatial data uniformly corrected with the new (January 1985) calibration data. The adjustment factors necessary to remove the variations among cameras (Table 5) are different than for the March 1984 calibration (Table 4).

The fact that the required gain adjustments are not the same for all bands within each camera indicates that spectral

calibration is also faulty. However spectral gain corrections will be considerably more difficult to calculate since there are 288 bands to be equalized instead of 8.

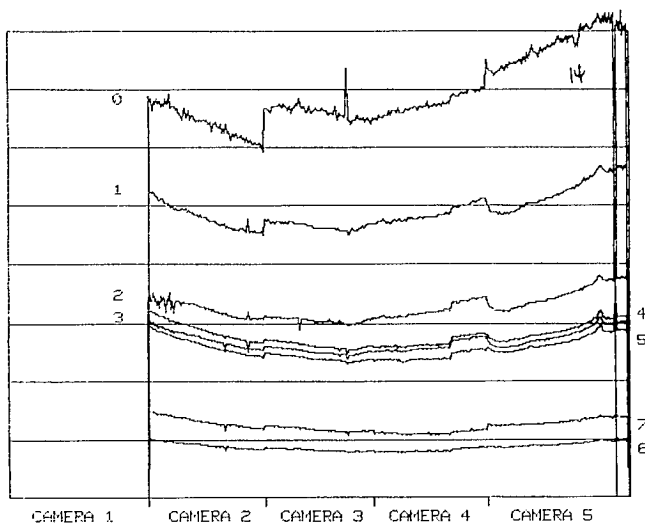


FIG. 14. Plots across the full swath of spatial image data acquired at 23,000' altitude just after the beginning of line 3, December 13, 1984 to illustrate the relative differences in signal level between cameras for different bands. The uniformity correction has been applied, but the additional corrections in table 5 have not. The increase in signal towards the edge of the swath is a result of increased path length. Correction for scan geometry is responsible for apparent differences in camera width. Camera 1 was not operational on the December mission.

TABLE 4. Camera Gain Adjustments required for June 1984 spatial imagery uniformity corrected with the March 84 Calibration data.

Spatial mode band	Diode range	Camera number				
		1	2	3	4	5
0	2-17	1.11	1.00	1.00	0.43	1.13
1	60-76	1.09	1.04	1.00	0.96	1.27
2	83-99	C	C	C	C	C
3	155-163	U	U	U	U	U
4	175-184	1.05	1.06	1.00	1.06	1.22
5	185-192	1.02	1.03	1.00	1.00	1.15
6	242-248	1.16	1.05	1.00	1.00	1.15
7	262-268	1.13	0.97	1.00	0.98	1.13

C = not calculated. U = unable to translate band 3 from HDDT.

TABLE 5. Camera Gain Adjustments required for December 1984 spatial imagery uniformity corrected with the January 84 calibration data.

Spatial mode band	Diode range	Camera number				
		1	2	3	4	5
0	23-35	N	1.10	1.00	1.00	0.96
1	84-91	N	1.05	1.00	0.99	1.00
2	119-126	N	1.02	1.00	1.00	0.99
3	155-163	N	1.02	1.00	1.00	1.01
4	175-185	N	1.02	1.00	1.00	1.00
5	186-196	N	1.03	1.00	1.00	0.97
6	213-217	N	1.02	1.00	1.02	0.99
7	242-251	N	1.03	1.00	1.04	0.98

N = not evaluated, camera 1 was not operational for December flights.

## 4.2. The Uniformity Correction

### 4.2.1. Spatial Mode Data

Blemishes on the arrays (groups of pixels which have non-linear properties) show up in spatial imagery as bad vertical columns in time, which either do not calibrate properly or are zero or 255. The worst of these “bad” spatial pixels are now avoided in the current IOS geometric correction procedure FLIGEO, which uses a look-up table to resample the imagery. However, a detailed examination of uniformity corrected spatial imagery is required in order to determine which pixels are being poorly corrected and correlate this with features in the calibration data. Some of the difficulty may be a result of the loss of precision due to band forming before diodes are summed or because of the current integer calibration. Other uncompensated variability may be due to the limitations of the current calibration data.

### 4.2.2. Spectral Mode Data

Blemishes are most noticeable in the spectral data if the band happens to include a row of spatial pixels which is

aberrant. In camera 3, band 3 is located over a group of low gain pixels; slow spectral mode band 7 overlaps a bad row on camera 5 (see Fig. 4); and camera 2 has two small blemishes which fall within band 3. Most of these non-uniformities are very small. We have not yet implemented corrective measures in the FLI calibration programs to avoid these blemishes, but slow spectral band 7 will have to be either “notched” or moved slightly.

### 4.2.3. Effect of Band Formation on Calibration of the FLI

Because of a limitation on data handling, not every diode on all five arrays can be recorded on every integration. The system is therefore designed to form 8 bands by summing off chip. While this contributes to better signal-to-noise performance, the need to sum pixel values within each band before applying dark and uniformity corrections has the effect of reducing the precision with which these gain and offset corrections can be applied, and reduces the precision of the uniformity correction. This will be most noticeable at low signal levels in regions of the arrays where the gains of neighbouring pixels are very different. Bands will have to be chosen to avoid these parts of the arrays.

## 5. EXAMPLES OF FLI IMAGE AND SPECTRAL DATA

### 5.1. Swath Width and Foot Print Size

The FLI swath width and foot print size will depend upon the solid angle subtended by each pixel and the aircraft altitude as well as the integration time and aircraft speed (which determine the smearing along-track). The June and December test flights were made at a variety of altitudes and speeds. By way of example, Fig. 15 summarizes the dimensions of spatial pixels with respect to altitude, aircraft speed and integration for the December mission. The aircraft velocity (and hence pixel length) increases with altitude, except where a headwind was encountered. Note that with the 90 ms integration times used for the December spatial mode operations the cross-track dimension was being over-sampled by a factor from 2 to 10 if square pixels were desired. The present IOS image display system only allows a  $512 \times 512$  image and if the analyst wishes to view the entire swath, the data must be subsampled by a comparable factor. The IOS geometric correction routine does this by skipping. However, if these pixels were averaged a further  $2 \times$  increase in signal-to-noise could be achieved.

### 5.2. Spectral data

Figure 16 illustrates a spectrum obtained during the December 1984 Chesapeake Bay mission. It was acquired over 'Slope Water' (a recognizable water mass of chlorophyll concentration and temperature intermediate between Gulf Stream and coastal water over the continental shelf of the eastern coast of North America) on line 9 from 500' altitude in the vicinity of station B1 on December 15, 1984. The spectrum is affected by solar sodium and hydrogen, and atmospheric oxygen and water vapour absorption lines at 590, 656, 687, 725 and 760 nm. In order to more directly compare this upwelling radiance spectrum with our previous work on *in vivo* fluorescence which has used reflectance

spectra, we have calculated a pseudo-reflectance spectrum. This was done by normalizing the upwelling spectrum to the spectrum of the incident light as seen by the sensor. With the IOS spectrometer, the incident signal is measured by viewing the sky and sun through an opal glass diffuser or by viewing a white panel of known reflectance to integrate sun and sky light. For the FLI data we do not have an up-looking spectrometer or a white reflectance panel. We have therefore used the spectrum of a thin cloud acquired on the same line as this upwelling spectrum. The cloud spectrum was obtained by difference, that is by subtracting the signal obtained over water from that obtained over the nearby cloud. The percent reflectance of the cloud is not known and therefore the water "reflectance" spectra cannot be expressed as percent. This calculation is not intended to be quantitative, but is to provide qualitative evidence that we are observing the same phenomenon as seen by Neville and Gower (1977), Gower (1980) and others.

The cloud "incident" spectrum clearly shows the water and oxygen absorption lines which also contaminate the upwelling spectrum from the sea. To a very large extent, these are removed in the "reflectance" spectrum, although differences in the depth or width of atmospheric absorption lines will show up as spikes in the "reflectance spectra" near the position of the lines. The chlorophyll fluorescence line is

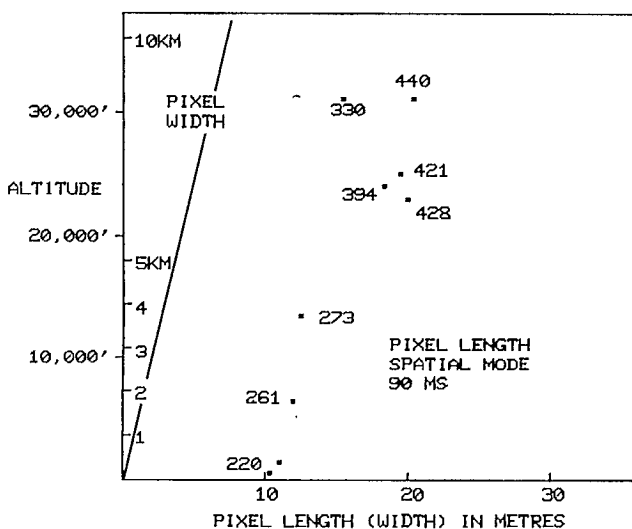


FIG. 15. The relationship between image pixel and swath width and pixel length with integration time, aircraft speed (in knots) and altitude for the December flights.

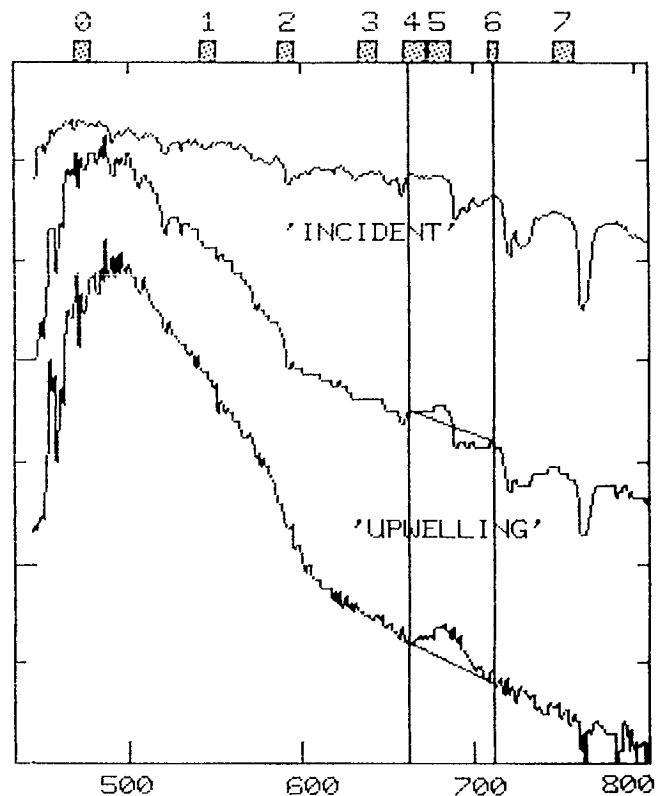


FIG. 16. A calibrated upwelling spectrum from off the east coast of Virginia, December 13, 1984 and the pseudo-reflectance spectrum calculated by normalizing it to the spectrum of the incident illumination. The incident spectrum was calculated by difference from data over nearby thin, low cloud. December spatial band definitions are shown along the top of the plot.

made clearly evident in the "reflectance" spectra and the baseline, above which a Fluorescence Line Height (FLH) is to be measured can then be chosen so that the end points avoid absorption features while still optimally measuring the fluorescence peak. Much of the noise on the "reflectance" spectrum results from the fact that the division done here was performed on the 8 bit video display system, not using the 16 bit data in memory. This figure also illustrates the spatial mode band definitions for the December mission and demonstrates how they were chosen to avoid absorption lines.

By comparison to Fig. 16, a family of spectra from the Eastern Township Lakes in Fig. 17 illustrates the observed change in spectra with increasing chlorophyll concentration. The *in situ* surface chlorophyll concentrations measured on the day of the flights or within 2 days are listed in Table 6. We have not yet calculated Fluorescence Line Height (FLH) values for this data, but the rise in the fluorescence peak is well demonstrated in spite of atmospheric absorption.

The Yamaska spectrum is interesting for two reasons. As well as exhibiting a large fluorescence emission with an apparent centre at 700 nm, this spectrum also has a peak near

650 nm. This "hump" can also be seen in reflectance spectra of outdoor phytoplankton cultures (Borstad unpublished data) and can be explained by the local minimum in absorption between chlorophyll *c* near 625 nm and chlorophyll *a* at 662 nm in natural phytoplankton (Lattimer and Rabinowitch 1957).

TABLE 6. *In situ* measurements from the Eastern Township Lakes, June 18–22, 1984 (McGill University Limnology Group).

Lake	Date sampled	Chlorophyll	
		0–1 m ( $\text{mg}\cdot\text{m}^{-3}$ )	Secchi (m)
Yamaska	19	24.2	0.6
Magog	22	3.5	2.1
Bowker	18	1.2	9.7
Lovering	22	1.3	3.4
Massawippi	22	2.1	2.5
Brompton	18	2.0	3.5

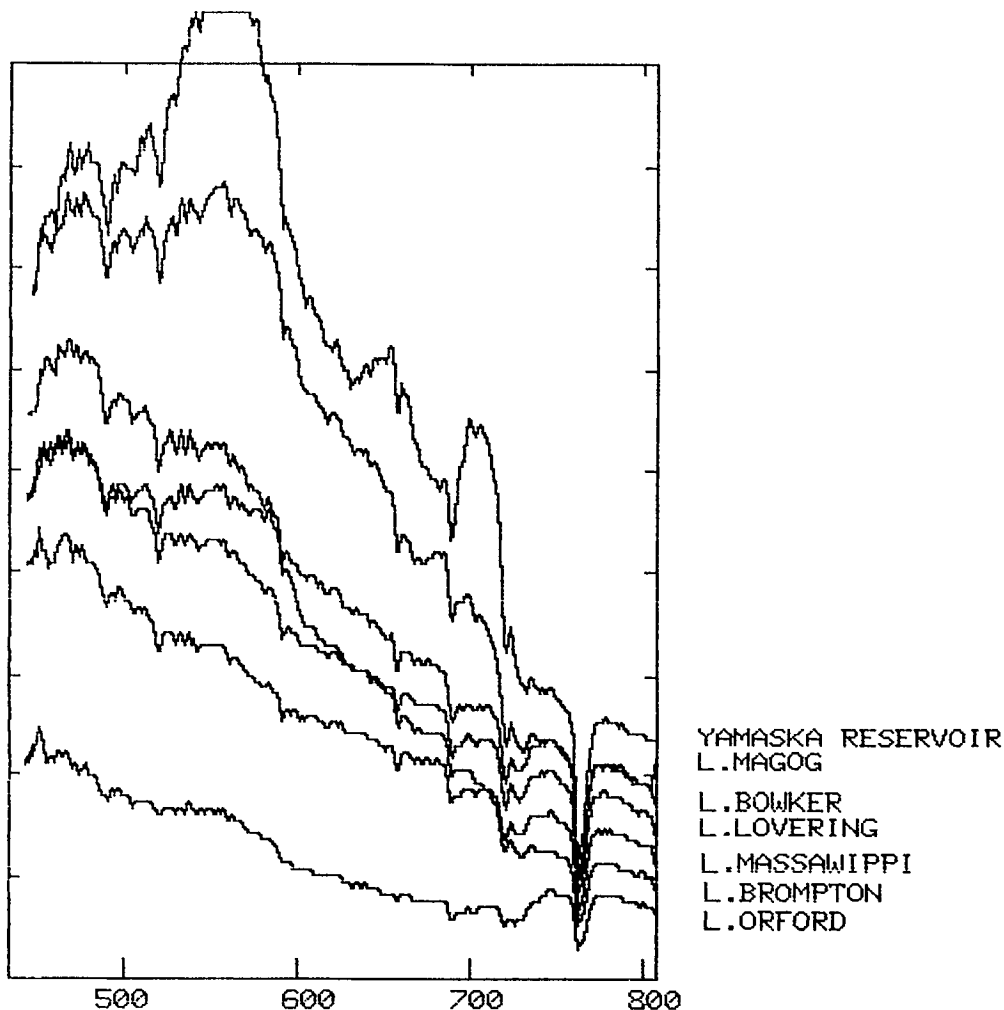


FIG. 17. A family of upwelling spectra from the Eastern Township Lakes, June 21, 1984 illustrating the increase in fluorescence line height with increasing chlorophyll concentration. [Yamaska Reservoir,  $24.2 \text{ mg}\cdot\text{m}^{-3}$ ; L. Magog,  $3.5 \text{ mg}\cdot\text{m}^{-3}$ ; others  $<2.1 \text{ mg}\cdot\text{m}^{-3}$ ]

The Yamaska spectrum also illustrates a phenomenon we have seen before in outdoor cultures of diatoms, eutrophic duck ponds with very high concentrations of planktonic green algae (Borstad unpublished data), and red tides of dinoflagellates or cryptomonad containing ciliates in coastal waters (Brown and Borstad 1982; Lin et al. 1984). This is the apparent shift of the fluorescence emission maximum to wavelengths greater than 688 nm. This is a result of self absorption caused by the overlap between the fluorescence and absorption bands and is also reported from laboratory work (Govindjee et al. 1973). The effective half-power band width of the chlorophyll *a* absorption at 670 nm is about 30 nm and therefore overlaps with the fluorescence emission line centred at 684 nm which has a half width of from 20 to 30 nm. The degree of reabsorption will depend on the relative size of the specific absorption and fluorescence coefficients for the algae being observed, and will depend on the species and physiological condition (Goedheer 1972). For diatoms, we have observed the shift at concentrations greater than about 15 to 20 mg·m<sup>-3</sup> of chlorophyll *a*, although we have now acquired spectra from the entire range of natural concentrations and many species. Greens, dinoflagellates and the ciliate-cryptomonad symbiont *Mesodinium rubrum* all seem to have larger absorption coefficients than their fluorescence coefficients, since the apparent FLH centre shifts to greater wavelengths at chlorophyll concentrations as low as 4 mg·m<sup>-3</sup>.

These differences in apparent peak centre wavelength are not as problematical for remote sensing as might appear. In data from over 20,000 km of reflectance spectra measured using the IOS spectrometer in Canadian and European coastal waters we have only seen a shift of the FLH peak from the range 680–689 nm where very high pigment concentrations or abnormal species are present, or in areas influenced by river runoff, where suspended inorganic sediments are the main colourant. The two situations can be easily differentiated on the basis of their overall reflectance and shape of the spectrum below 650 nm. In red-tide situations where the peak shift is due to increasing pigment concentrations, we have been able to use the simple 3 point FLH calculation to quantitatively measure *in situ* chlorophyll (Brown and Borstad 1982; Lin et al. 1984), however it was necessary to use wavelengths optimized for the shifted peak.

Figure 18 illustrates another previously unreported phenomenon discovered in the June FLI data. Spectral data of some of the Eastern Township (E.T.) Lakes show an asymmetrical "peak" in the vicinity of 708 nm. It is our opinion that this is evidence of benthic plants, and that the peak is formed by the interaction of chlorophyll reflectance which has a high shoulder near 710, and water absorption which is strongly increasing toward long wavelengths. We have duplicated this phenomenon in the laboratory using leaves submerged under increasing depths of water (Gower and Borstad, unpublished data).

This 708 nm "peak" is only found in FLI data for some of the E.T. lakes and then only near the shore or in shallow bays, where aquatic plants are plentiful (Dr. J. Kalff, McGill University; personal communication). The spatial distribution of this feature in Lake Massawippi can be seen in Fig. 19. This "spectral image" has been constructed from spectral mode data by calculating a difference between the upwelling signal at 708 nm and 721 nm for each of the 8 bands in all 5 cameras. The image is only 40 pixels wide and spatial resolution is poor, however it demonstrates the power of the FLI to

detect and image the spatial distribution of fine spectral detail.

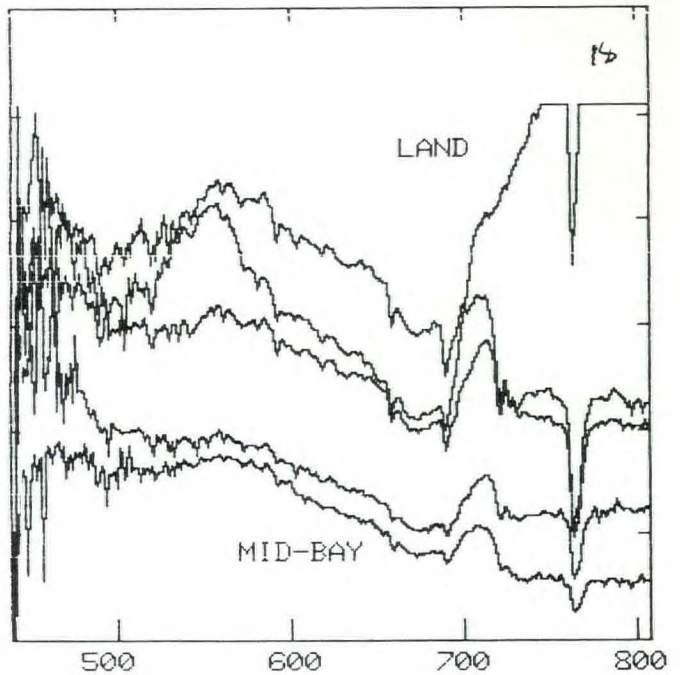


FIG. 18. Upwelling spectra from along a line crossing the shore of a small shallow bay in Lake Massawippi. The radiance peak at 708 nm is interpreted as interaction between the strongly increasing water absorption and the red reflectance shoulder from chlorophyll in benthic plants.

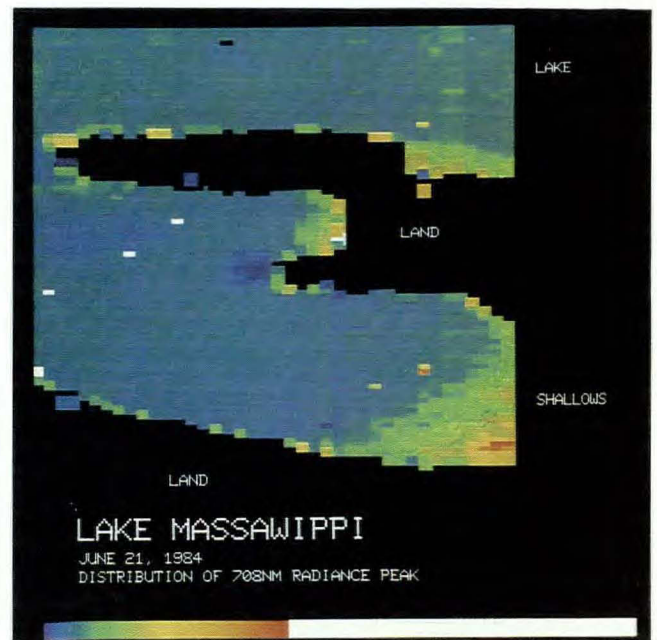


FIG. 19. A spectral image of the 708 nm radiance peak in Fig. 18 illustrating the areal distribution of this phenomenon in Lake Massawippi.

Figure 20 illustrates a third long wavelength phenomenon seen in FLI spectral data from Lake Massawippi, which is not yet fully analysed. Spectra obtained over some parts of the this lake and on the Lake Ontario flight line show a progressive increase with approach to the shore. However, in this case there is a constant increase with wavelength and a "peak" is not formed. The most probable explanation involves leaves and stalks of emergent vegetation covering a fraction of the IFOV of the sensor. Figure 21 is a spectral image illustrating the distribution of this phenomenon in the region surveyed. The distribution along the lake edge supports the explanation in terms of aquatic vegetation.

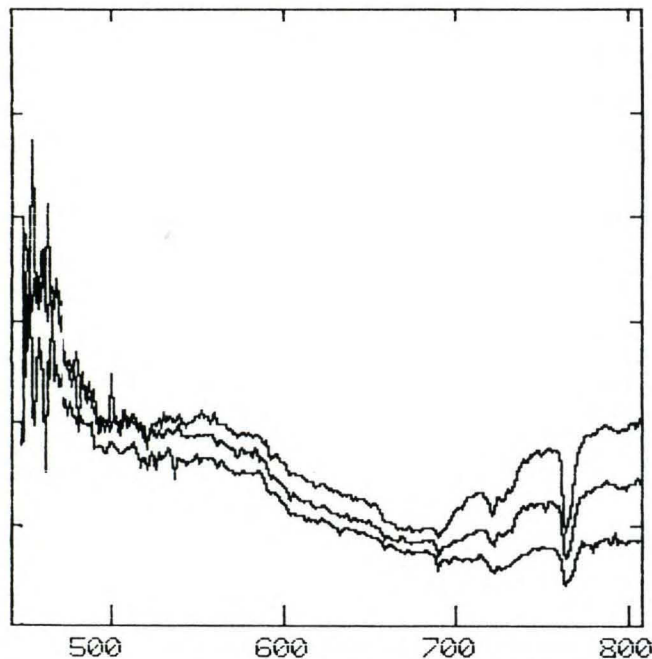


FIG. 20. Upwelling spectra from near the shore of Lake Massawippi showing a progressive increase in red reflectance near shore, probably due to emergent aquatic vegetation.

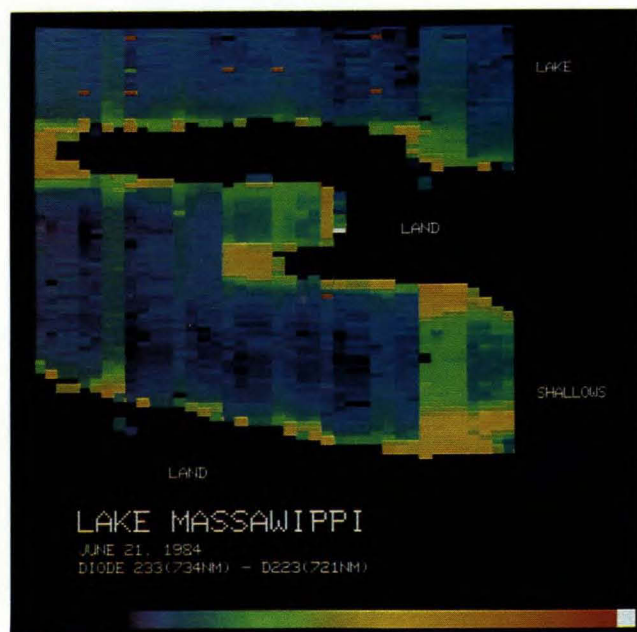


FIG. 21. A spectral image of Lake Massawippi showing the red reflectance increase illustrated in Fig. 20.

Figures 22 and 23 show examples of FLI slow spectral data obtained from 500' altitude along line 7 on December 13, 1984. This line began over the very turbid, bright brown waters in Pocomoke Sound and continued over clearer green-blue coloured waters of Chesapeake Bay. The three indices plotted in Fig. 23 demonstrate the variation of a green to blue

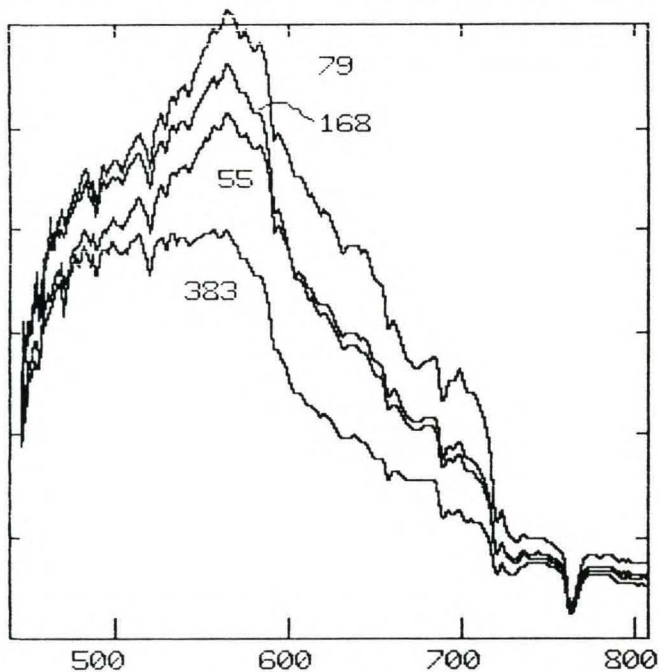


FIG. 22a. Upwelling spectra from along line 7 in Pocomoke Sound, December 13, 1984 showing variation caused by differences in sediment and chlorophyll content. Numbers on spectra are to be used to locate the spectra along the plots in Fig. 24.

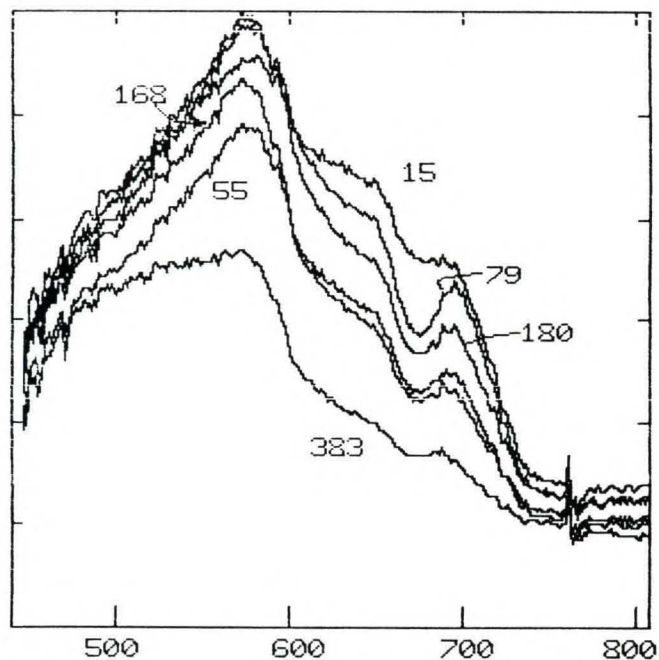


FIG. 22b. "Reflectance" spectra corresponding to positions along line 7 in Pocomoke Sound, December 13, 1984. Variations in spectral shape are due to differences in sediment and chlorophyll content.

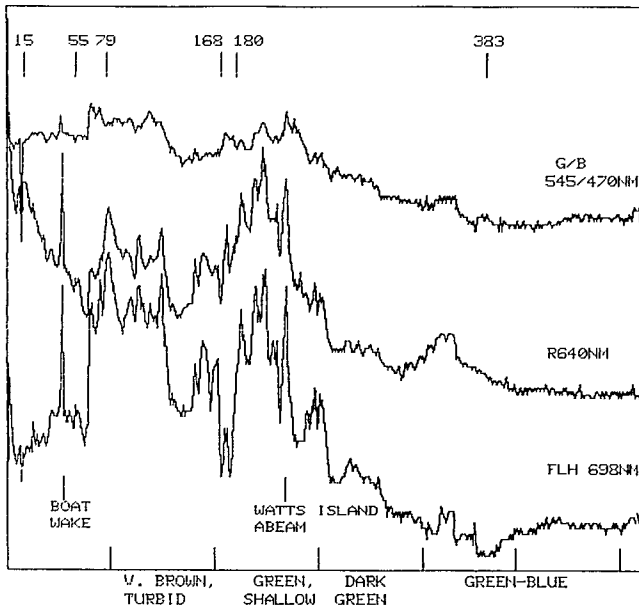


FIG. 23. Variations of water colour indices along line 7 in Pocomoke Sound and Chesapeake Bay, December 13, 1984 calculated from band 0 camera 3 spectral data obtained from 500' altitude.

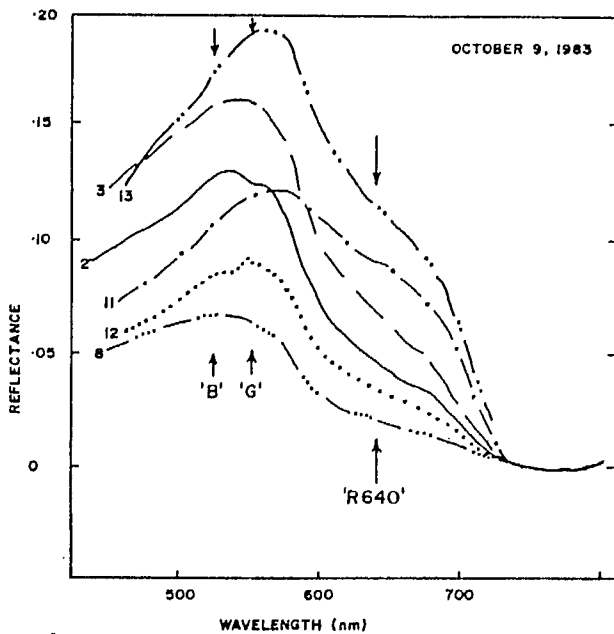


FIG. 24. Reflectance spectra of turbid waters of the Beaufort Sea obtained with the IOS spectrometer, October 9, 1983 (Borstad 1985).

ratio (545/470 nm), upwelling radiance at 640 nm (as a measure of turbidity or brightness), and Fluorescence Line Height (FLH) centered at 698 nm. Comments extracted from flight notes of visual observations are noted along the bottom of the plot.

Past data have shown that our simple three point Fluorescence Line Height measure is artificially elevated by increases in inorganic Suspended Particulate Material (SPM), Borstad et al. 1980; Borstad 1985) and there is also evidence of this here. Nevertheless, the shape of the spectrum indicates a large phytoplankton population in Pocomoke Sound. Com-

pare the spectra from Pocomoke Sound with those in Fig. 24 which were obtained with the IOS spectrometer in the Beaufort Sea in 1983 (Borstad 1985). The chlorophyll concentrations for the Beaufort stations were all less than  $1 \text{ mg m}^{-3}$  and the change in shape of the reflectance spectra with increasing SPM is clear. In that data, a simple comparison of reflectance at 640 nm with SPM showed good agreement and R640 was used to map SPM. The FLI reflectance spectra obtained over Pocomoke Sound show a similar increase below 700 nm, but also have a strong dip at 670 nm due to absorption by chlorophyll *a*. No *in situ* information is yet available, but the Sound is known to support large populations of blue-green algae.

The FLH, R640 and G/B do not co-vary everywhere along the flight track. Difference spectra were calculated for line 7 by subtracting one spectrum from another on the 8 bit display system (Fig. 25). The spectra which are the result of differential backscatter and absorption between the two locations are consistent with decreasing sediment and chlorophyll concentrations along the line.

No spectral images can be made from the Chesapeake Bay data at this time because not all FLI bands were stripped when the data was translated from High Density Digital Tape (HDDT). In the limited time available it was decided to translate only 1 or 2 bands from each flight line, to enable a longer section of flight data to be packed onto each 2400' CCT.

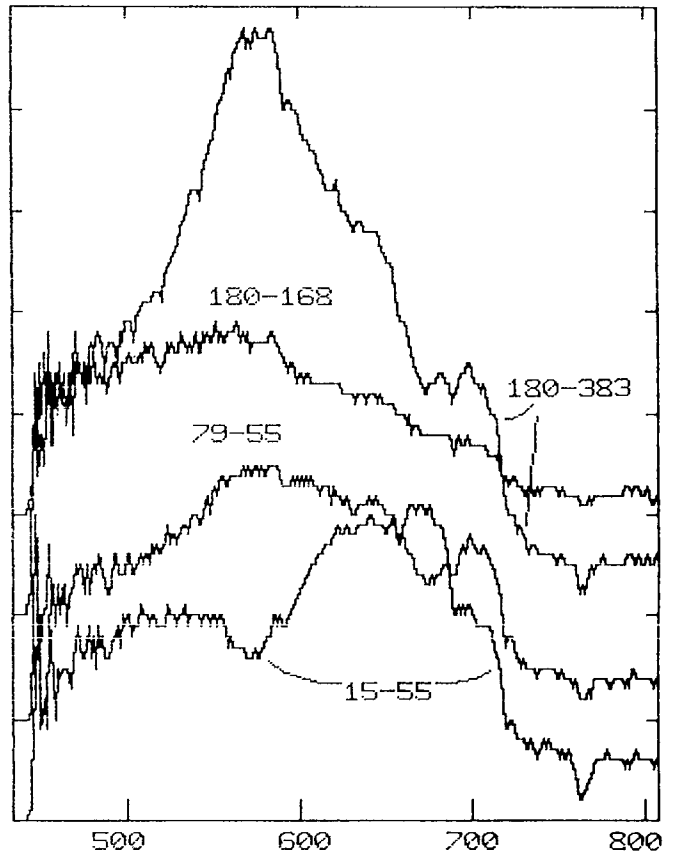


FIG. 25. Difference spectra from along line 7 over Pocomoke Sound and Chesapeake Bay, December 13, 1984.

### 5.3. Spatial data

In the spatial mode, the spatial resolution is much greater than the 40 pixel wide images shown above, since the full 1925 pixel swath is available in 8 bands. An 8 pixel overlap between cameras, non-uniformities across the spatial dimension of the arrays and differences between camera

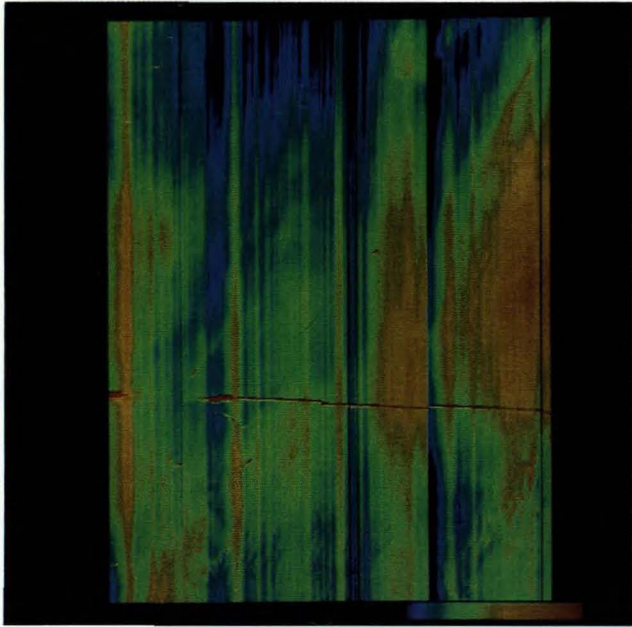


FIG. 26. Raw uncalibrated band 5 spatial imagery from line 3, December 13, 1984 over the Chesapeake Bay Bridge-tunnel. Corrected for scan geometry only. Vertical striping is caused by non-uniformities on the arrays.

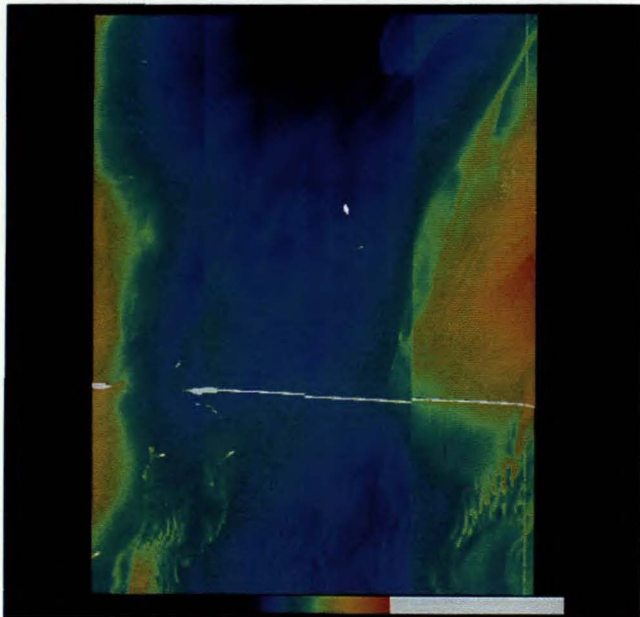


FIG. 27. Band 5 spatial imagery from line 3 December 13, 1984. Same scene as Fig. 26 with uniformity correction but without camera gain adjustments, radiometric correction for atmospheric effects or correction for camera mis-alignments.

gains are removed during data processing. By way of example, Fig. 26 illustrates an uncalibrated band 5 (673-687 nm) image acquired over the mouth of Chesapeake Bay on December 13, 1984. No land is visible in the image, but the Chesapeake Bay Bridge-tunnel can be seen crossing the middle of the image. Gain non-uniformities in each array and between cameras are responsible for the vertical along-track striping.

This striping is largely removed by the uniformity correction (Fig. 27) and the camera gain adjustments (Fig. 28) referred to in section 4.1.2. above. However, blemished pixels or those with non-linear gains and offsets very different from their neighbours will not be corrected in our present single point gain calibration. Further, the full resolution image in Fig. 29 shows that not all of the poorly calibrated spatial pixels are related to identifiable blemishes on the calibration data. This may mean that rounding errors in the integer calibration may be responsible.

The uniformity corrected imagery in Fig. 28 has not been corrected for atmospheric effects, and these can be seen as limb-brightening as the path length increases towards each edge of the swath. This is also evident in the graphics plot across the beginning of this image (Fig. 14). This atmospheric correction will be the next step in correcting the FLI data, but for the purposes of this report, these effects can be grossly removed by setting the average of each vertical column in the image to the average for the entire image. The result is that the image is "flattened" radiometrically and considerable in-water structure is made visible (Fig. 30). Several vessels and their wakes can also be seen.

In this scene the radiance increased across the entire spectrum (Fig. 31) and a similar spatial pattern could be seen in all spectral bands. It was probably therefore not due to phytoplankton variations. A uniform increase could be the result of illumination changes, however the pattern of the

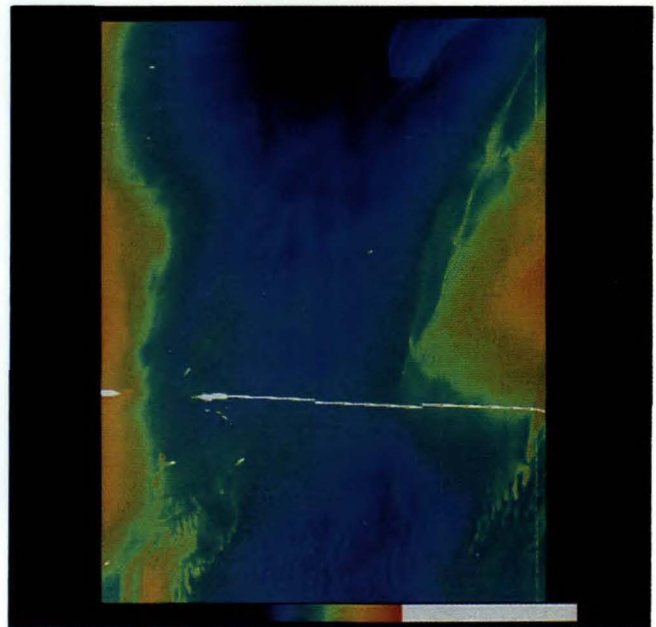


FIG. 28. Band 5 spatial imagery from line 3 December 13, 1984. Same scene as Fig. 27 but with camera gain adjustments.



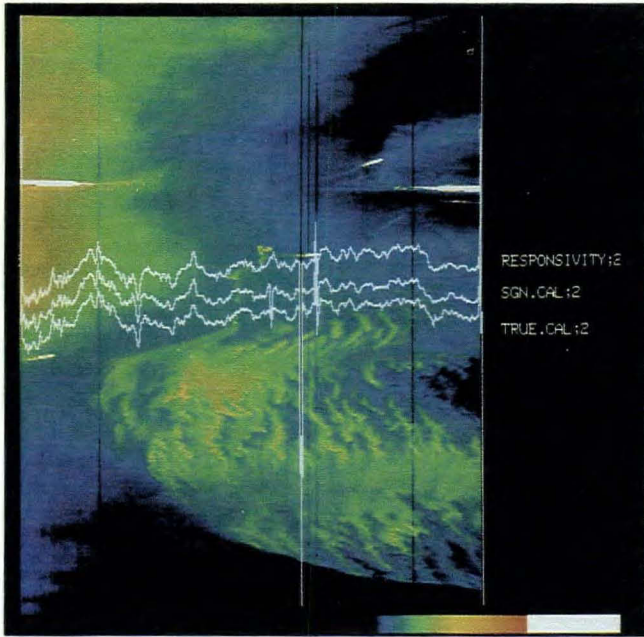


FIG. 29. A full resolution portion of the uniformity corrected band 5 spatial imagery in Fig. 27, showing the tunnel section of the Chesapeake Bay crossing. Plots of the spatial variations of the calibration data in that band are superposed in white. Most of the structure on the arrays, has been mapped in the calibration and is well compensated for, but some vertical striping on the imagery does not coincide with blemishes.

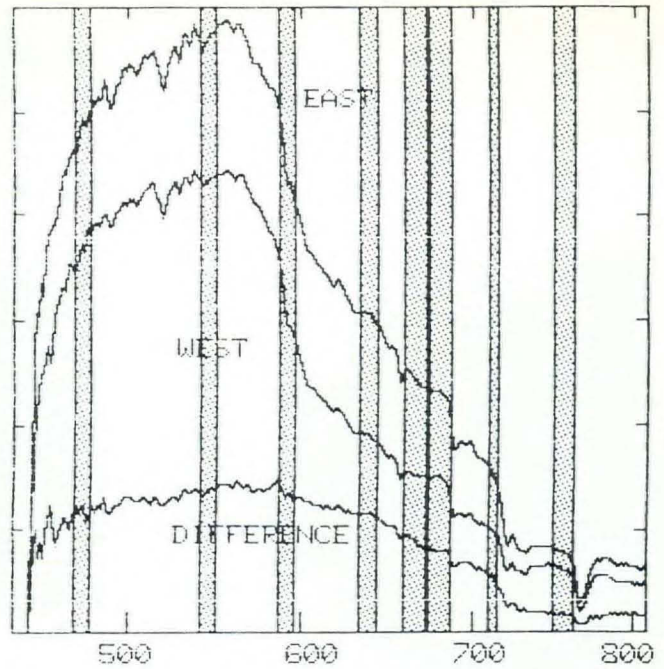


FIG. 31. A pair of upwelling spectra from line 3, December 13, 1984 approximately 1 km on either side of the Chesapeake Bay bridge-tunnel (shown in Fig. 26–30). The lower plot shows that the radiance difference between the two areas was uniform spectrally. The radiance variations in the spatial imagery in Fig. 25–30 are therefore probably due to inorganic sediment load.

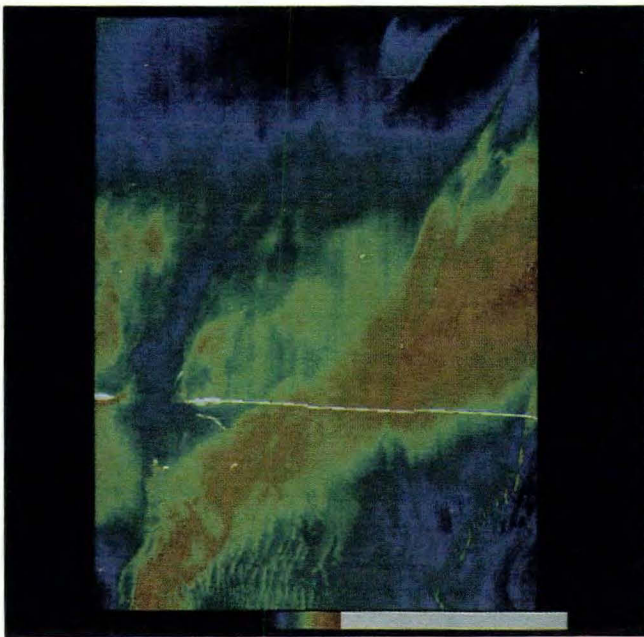


FIG. 30. Band 5 spatial imagery from line 3 December 13, 1984 with geometric, uniformity, and camera gain corrections applied (same scene as Fig. 26, 27, and 28), but with the sum of each vertical column set to the average of the columns for the entire image. This has the gross effect of radiometrically "flattening" the image and very roughly approximates an atmospheric correction, revealing considerable in-water structure.

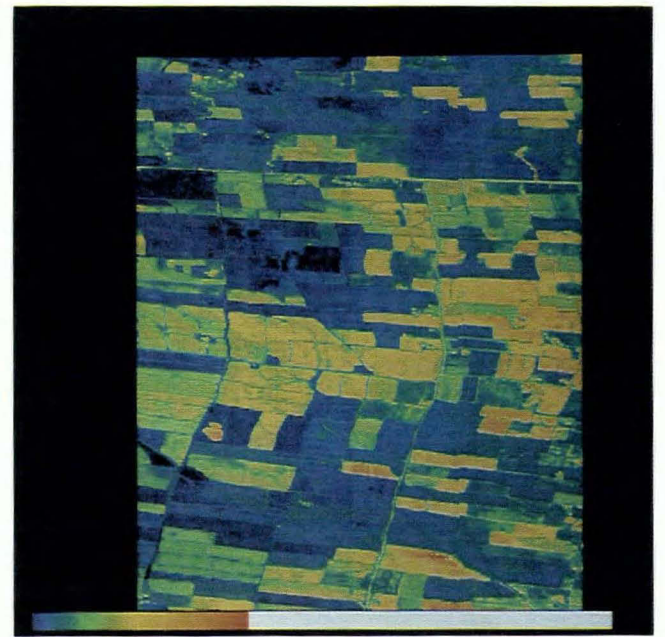


FIG. 32. A full swath band 2 (540–560 nm) spatial image of an agricultural area near Winchester Ontario, on June 22, 1984. Uniformity corrections and empirical camera gain adjustments have been applied. No attitude information was available on this flight and therefore aircraft roll is not compensated for.

radiance increase suggests it was caused by in-water variations, possibly of inorganic sediment. Surface *in situ* data not available at the time of writing may help to resolve this question.

Two of the June flights were over land targets. Figure 32 is a full swath, geometrically corrected band 2 image (540–560 nm) acquired from 9500' altitude over an agricultural area near Winchester, Ontario. The uniformity correction, camera gain adjustments and empirical limb-brightening correction referred to above have been applied. No navigation or aircraft attitude data was available on this flight and no roll correction has been made. Because the scene was too bright to be imaged using the full-open aperture, the cameras had to be stopped down and integration times increased. This data was therefore obtained at 300 ms which created an along-track smearing on the order of 18 m. When it was delivered the two possible iris settings for the FLI were in a ratio of 35:1. The large difference proved to be too great and this has since been changed to 8:1.

Figure 33 illustrates a portion of a full resolution image obtained from 23,000' over Norfolk, Virginia. The uniformity, cross-track geometry and limb-brightening corrections have been applied. The outline of the subdivisions in the city can be seen and a racetrack is visible near the top of the image. Misalignments between cameras 2 and 3 are visible about a quarter of the width from the right side of the image.

Figure 34a is a colour composite taken over Renfrew, Ontario, during the most recent series of test flights in July 1985. The data is unedited and is presented at full resolution. It illustrates successful use of the in-flight uniformity correction based on an earlier calibration. An expanded section (Fig. 34b) of the same image shows the area of overlap

between cameras. The jog in the roadway is an artifact of the overlap. Figures 35a and b show the effect of removing this overlap and of removing line dropouts present in the raw image.

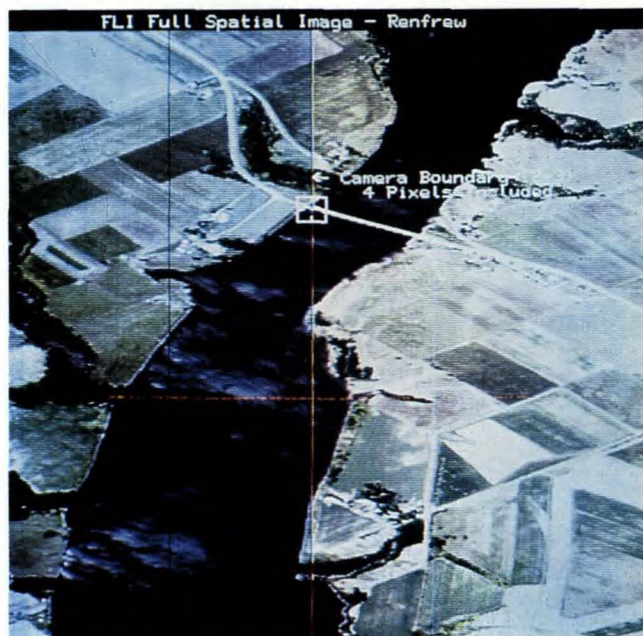


FIG. 34a. Colour composite of full resolution spatial imagery over Renfrew, Ontario. Real time uniformity correction has been applied. Vertical lines illustrate array blemishes and horizontal lines are due to transcription errors.

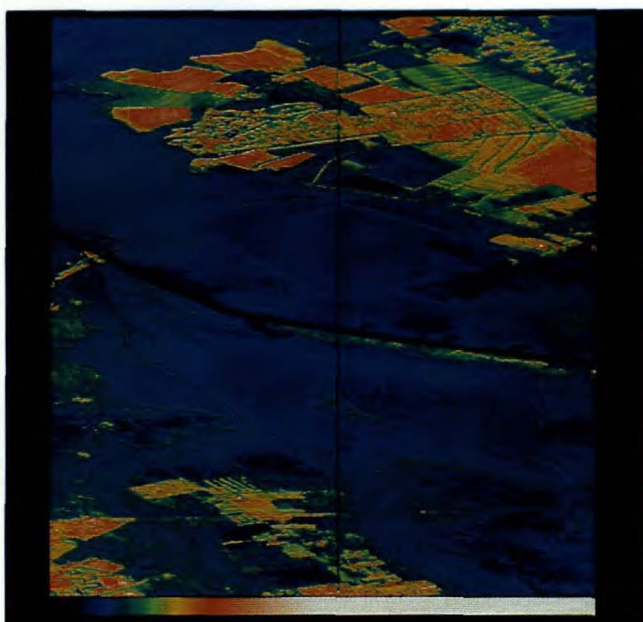


FIG. 33. A portion of full resolution band 2 spatial imagery over Norfolk, Virginia acquired December 14, 1984 from 23,000'. Uniformity and camera gain adjustments, and cross-track (scan angle) geometric corrections have been applied.



FIG. 34b. The same as in Fig. 34a but expanded by a factor of 2 about the cursor. The expanded area shows the effect of overlap and poor array performance near each edge.



FIG. 35a. Edited colour composite over Renfrew, Ontario, July 1985. As in Fig. 34 but removing the overlap between camera array blemishes and transcription errors. Although the cursor is not shown it is positioned in the same place as in Fig. 34a.



FIG. 35b. The same area as in Fig. 35a but expanded by a factor of 2 about the cursor position.

## 6. CONCLUSIONS

It appears that most of the original goals of the instrument design have now been met. As well as producing spatial imagery similar to other devices currently in use, the Fluorescence Line Imager has admirably demonstrated its flexibility by being reprogrammed several times to change the position and width of the spectral bands. It has also produced high spectral resolution data over both water and land targets and this data has been used to create "spectral images" of very narrow spectral features which are not available from any other sensor currently in use. Chlorophyll fluorescence has been detected as a narrow peak in the vicinity of 685 nm and a previously undescribed spectral feature near 700 nm has been detected and mapped with spectral imaging. The high spectral resolution and the general flexibility of the instrument give the FLI a very significant advantage.

The instrument can probably now be considered operational, in spite of the fact that it is still a prototype. Most of the problems encountered with the instrument have been related to the fact that a "bread-board" instrument was not built first and faults or inadequacies had to be discovered through operational testing. Work on the instrument since its delivery has improved its performance considerably and the collective experience with the instrument and the data it produces has shown that further improvement can be expected.

The optical response at short wavelengths is less than had been originally hoped, but is similar to what can be expected from EEV P8600 arrays and the optics used in the FLI. Use of other more recently available arrays could significantly improve the instrument performance.

Several blemishes are present on the EEV arrays used in the FLI, and the effect of these can be seen in spectral and spatial mode image data from some bands. The location of these blemishes is easy to determine however, and for the most part they can be avoided by notching or placing bands so as to avoid them.

Fixed pattern and random noise were severe in some cameras on the June flights, but appear to have been reduced by engineering alterations performed during 1984. As of December, 1984 the read-out noise floor in laboratory data was nearly equal to the array manufacturers specifications and the system signal to noise ratio was dominated by shot noise above about 1/13 of full scale. Flight data still shows higher noise.

Alignment and calibration of the five FLI camera modules remains a problem. The cameras must occasionally be removed from their mounting in the FLI for adjustment or repair, but tolerances are small and it is impossible to reinstall them in exactly the same position. A time consuming and therefore expensive re-alignment is necessary each time the camera modules are worked on. This aspect of the instrument design should be carefully evaluated when the next generation of the FLI is constructed.

Image data calibrated with the March 1984 calibration data showed gross differences in digital level between cameras which were thought to have been caused by variation of the calibration lamp during the exercise. However, in spite of elaborate precautions to stabilize the calibration lamp outputs during the January calibration, the resulting uniformity correction does still not fully correct for gain differences

between cameras. We have empirically remedied this problem using gain adjustment factors, but an absolute radiance calibration for all five cameras is impossible until the cause of these differences is found and corrected.

In order to avoid overflow of the 16 bit integer arithmetic now used in the calibration procedure, the uniformity correction is calculated as a binary fraction which is used to reduce the numerical value of the raw signal. Because of the large variation of spectral sensitivity of the arrays, the uniformity correction varies over a factor 80 across the spectrum. In the integer calculations now used, the arithmetic precision is near 16 bits at short wavelengths where the PCF is near unity, but considerable precision is lost in the region of the fluorescence signal. This procedure should be replaced with floating point calculations performed on a larger computer.

The Fluorescence Line Imager produces a prodigious amount of data and this has presented some problems in trying to analyse it on a small time-shared computer. Only a fraction of the data from the June and December flights has now been analysed and the performance of the instrument has not yet been fully evaluated. This is not possible using field data alone, and controlled lab experiments are necessary for a more complete engineering evaluation.

The spectral data of lakes and the ocean obtained from the Fluorescence Line Imager behaves as predicted from our experience with the IOS spectrometer. In spite of the loss of considerable precision in the vicinity of the fluorescence line (caused by the present integer calibration procedure), FLI spectral data from the Eastern Township Lakes shows a variation in the height of the fluorescence line at 685 nm which is in agreement with measured *in situ* variations of chlorophyll *a*. We have also been able to repeat our earlier observations made with the IOS spectrometer, that spectral data from very eutrophic waters show a peak shift to wavelengths greater than 685 nm. By artificially constructing an "incident" spectrum from spectral data obtained over a white cloud, we have also been able to calculate a reflectance spectrum very similar to those calculated with the spectrometer.

Data from the June and December missions have demonstrated the unique capability of the FLI to provide complementary spectral and spatial information which greatly assists in interpretation of observed features. In June we were able to detect and then image a previously unsuspected radiance peak at 708 nm in spectral data from Lake Massawippi. The distribution of the phenomenon in spectral imagery suggested that the feature was caused by interaction between water absorption and chlorophyll reflectance from submerged benthic plants. This was confirmed by simple modelling.

Spatial imagery obtained on both the June and December flights demonstrates the imaging capability of the sensor. Two of the June flights acquired imagery over land, which is being analysed by scientists in other disciplines. An improved geometrical alignment and the utility of the real-time calibration system have been demonstrated during the July 1985 hydrographic mission.

Spatial image data over water at the mouth of Chesapeake Bay on the December mission showed complex

structure just seaward of the Bridge-tunnel. This structure was visible in all bands and spectral differences calculated over the feature demonstrated that the feature was caused by

inorganic sediment. We expect to see clearer effects of phytoplankton pigments in the July 1985 data when this is analysed.

## 7. RECOMMENDATIONS

### A — The FLI development program

Most of the original goals of the FLI instrument design have now been met, and the present instrument is gathering data in an operational manner. Canadian industry has established an important lead in the technology of CCD array spectral imaging for remote sensing, and this lead and the momentum generated should not be lost. Development of a space version should be started, with various aspects of the improved design being tested on the present instrument. A program of supporting experimental measurements is also needed.

### B — The present FLI instrument

#### 1. Noise sources

Several sources of noise in the FLI data have been removed or greatly reduced, but noise that appears to come from electronic pick-up is still limiting important aspects of instrument performance. These noise sources should be located and removed. The analog to digital converters should be replaced with units adjusted to correct the anomalous response.

#### 2. Wiring and mechanical improvements

The present FLI instrument is not particularly robust. It has evolved rapidly through mechanical and electronic changes which have not helped this situation. Broken wires have caused several delays, and poor lay-out may be contributing to noise pick-up. Corrosion has been noted close to the CCDs, possibly related to moisture build-up. A re-evaluation of the air drying system and a moderate amount of general reworking and ruggedizing should be carried out to produce a more compact and reliable system.

#### 3. System crashes

The system crashes that still periodically interrupt data collection, need to be investigated and cured. These may be related to the need for improved wiring and layout or to the moisture build-up, as noted above, or may be a purely software problem.

#### 4. Real-time display

Real-time display of FLI image and spectral data is needed in the aircraft to allow better monitoring of the instrument and the data collected during flights.

#### 5. Data recording

Quality of data recording on the HDDT and its subsequent retrieval, is critical to the success of the instrument. The cause of the "bad scanlines" in the June and December flight data should be investigated in more detail. The modifications to the HDDT interface by CCRS have not completely solved the problem.

#### 6. Near real time calibration data analysis

An alteration to the current calibration routine and/or computer should be considered which would permit real-time

or near real-time analysis of the data obtained. The acquisition of calibration data onto diskette and analysis of the data days or weeks later is highly inefficient. In data from both the March 1984 and January 1985 calibrations problems such as a sticking shutter (causing light leaks), saturated pixels, regions of zero input have been seen. Some of these could have been quickly and inexpensively remedied if the situation could have been detected at the time of calibration. Use of a larger computer would solve many of these problems.

#### 7. Improved CCDs

7.1. The performance of other CCD devices should be investigated, with a view to ultimately improving the blue response of the FLI by replacing the EEV P8600 arrays now being used. The current low blue sensitivity of the P8600 arrays is useful for high altitude measurements since it tends to equalize the measured signal across the array. However it will be impossible to obtain equal precision across the spectrum as long as there is a very large difference in radiometric sensitivity across the array.

7.2. In a second generation instrument, efforts should be made to obtain CCDs which are matched and blemish-free if this is possible.

### C — Analysis of FLI data

#### 1. Calibration

##### 1.1. New software

A new version of the IOS calibration routine should be written to perform the calibration in floating point arithmetic instead of integer. The full precision could therefore be retained across the spectrum since fractional scaling factors (now required to avoid overflow) could be eliminated. The program should be a one-step operation and use Band Correction Factors calculated at the time of processing and for the data in question rather than requiring Band Correction Files to be calculated and stored separately for every band definition. The current procedure does not allow the operator to easily switch between data types (different band definitions or iris settings), because only one set of BCF.CAL's are stored. (This has been written and is now in use as of June 1985.)

##### 1.2. Variations between cameras

The observed spectral and amplitude variations in calibrated output among cameras should be investigated in some detail. This may represent variations in lamp output, variations in attaching the cameras to the calibration sphere, or change in the behavior of the arrays with time.

##### 1.3. Improved radiance calibration technique

1.3.1. If the FLI calibration could be carried out using a HDDT to record the data instead of diskettes, then the various error sources that are presently degrading this data could be analysed, and a more accurate calibration at all wavelengths could perhaps be achieved. Recording the data on tape would also allow detection of time variation of the calibration lamp and removal of noise introduced at this stage.

1.3.2. If calibration data can not be recorded on tape, consideration should be given to performing a two-stage

calibration of the instrument. This would be an extension of the January calibration exercise but using a very dark blue filter in combination with long integration times to obtain a precise calibration of the lower half of the arrays only. This calibration could later be mathematically "spliced" to calibration data for the upper part of the array using the image processor. It may also be possible to work backwards from field data (for instance the altitude difference spectra) to adjust the uniformity correction at the bluest wavelengths.

#### 1.4. Scattered light evaluation

The shape of spectral data collected with the FLI at wavelengths less than 480 nm suggests that a significant error is introduced by scattered light in the instrument. This should be evaluated and corrected, either in the instrument or in data processing.

#### 1.5. Blemishes

The blemishes and pixels on the present arrays for which gain and offset variations are uncorrectable should be systematically mapped and all bands moved or notched to avoid them.

#### 1.6. Dark data analysis

As part of on-going evaluation of the FLI, dark data obtained during the December 1984 flights should be translated and analyzed to look for variations in dark level during each flight, and to analyse the statistical properties of the observed noise and their variations with time.

### 2. Geometrical corrections

#### 2.1. Improved software

The current FLI geometric correction program at IOS is a first approximation and should eventually be improved. This has not been a high priority, but for mapping applications over land it will become critical. Roll corrected geometry using inertial navigation data will also be necessary.

#### 2.2. Improved optical characterization

If more complete optical performance evaluation of the FLI is desired (for instance Modulation Transfer Function), laboratory measurements will be required. This characterization is probably not required for this stage in the development of the system for water imaging but will become important if the FLI is to be used for highly accurate spatial mapping (bathymetry or of land targets).

### 3. Analysis of flight data

The test data from the June and December flights are only partly analyzed. Electronic noise on the June flights will limit the amount of time that can profitably be spent on this data, but some useful information from these flights remains unanalyzed. The December data is of much better quality and

should be examined in some detail, particularly since this was designed to be a comparison of active laser stimulated and passive solar stimulated fluorescence detection techniques. No comparisons have yet been made, either to the laser results or to in situ observations made by Bedford scientists operating on the CSS *Hudson* offshore or by the Maryland and Virginia state health authorities who were sampling in Chesapeake Bay itself. No ground truth has yet been obtained.

### 4. Modelling and experimental measurements

The fluorescence signal and the optical interactions in that region of the spectrum are not completely understood. A mathematical model should be constructed to provide the framework for fieldwork designed to, among other things, investigate the effect of inorganic suspended material on the fluorescence signal. The apparent shift of the FLH signal to longer wavelengths as chlorophyll concentrations increase and for certain types of phytoplankton should also be investigated.

## D — Operation of the FLI instrument

### 1. In flight parameters

The system parameters (camera aperture and gain, integration time) which along with aircraft altitude and velocity determine the shape of the ground-projected footprint and along track smearing should be examined to determine the optimum operating conditions.

### 2. Signal level

The FLI should be operated and calibrated at signal levels as near to saturation as possible, in order to obtain maximum signal-to-noise. Problems of incipient saturation should be investigated, such as the grid pattern on cameras 1 and 2 at high signal levels.

### 3. Camera equalization

Camera 4 presently has a very different response from the other cameras. Its much higher sensitivity below about 600 nm means that in order to avoid saturation on this camera, the other cameras must often be operated well below their full well limit with the result that signal-to-noise is not optimal. Consideration should be given to adjusting the gain of camera 4 to more closely approximate that of the other four in the blue-green part of the spectrum. (This was adjusted as recommended in July 1985.)

## 8. REFERENCES

- ARVESEN, J. C., J. P. MILLARD, AND E. C. WEAVER. 1973. Remote sensing of chlorophyll and temperature in marine and fresh waters. *Astronautica Acta* 18: 229-239.
- BØLVIKEN, B., F. HONEY, S. R. LEVINE, R. J. P. LYON, AND A. PRELAT. 1977. Detection of naturally heavy-metal poisoned areas by Landsat 1 digital data. *J. Geochem. Explor.* 8: 454-471.
- BORSTAD, G. A.. 1985. Water colour and temperature in the southern Beaufort Sea: remote sensing in support of ecological studies of the bowhead whale. *Can. Tech. Rep. Fish. Aquat. Sci.* 1350: 69 p.
- BORSTAD, G. A., R. M. BROWN, AND J. F. R. GOWER. 1980. Airborne remote sensing of sea surface chlorophyll and temperature along the outer British Columbia coast. *Proc. 6th Can. Symp. Remote Sensing, Halifax 1980*, p. 541-547.
- BORSTAD, G. A., R. M. BROWN, D. TRUAX, T. R. MULLIGAN, AND J. F. R. GOWER. 1981. Remote sensing techniques for fisheries oceanography: examples from British Columbia. *NAFO Sci. Coun. Studies* 4: 69-76.
- BORSTAD, G. A., AND J. F. R. GOWER. 1984. Phytoplankton distribution in the eastern Canadian Arctic. *Arctic* 37: 224-233.
- BROWN, R. M., AND G. A. BORSTAD. 1982. Chlorophyll *a* determinations from solar stimulated *in vivo* fluorescence. Unpubl. report by Seakem Oceanography Ltd. to Dept. Fisheries and Oceans, Sidney, B.C., DSS contract OSB81-00108, 230 p.
- CCUSS. 1981. Investigation of the Feasibility of Mapping Chlorophyll Fluorescence from Space. Report by the Canadian Consortium for University Space Science for the Department of Fisheries and Oceans, March 1981, 173 p.
- CLARKE, G. L., G. L. EWING, AND C. J. LORENZEN. 1970. Spectra of back-scattered light from the sea obtained from aircraft as a measure of chlorophyll concentration. *Science* 167: 1857-1866.
- COLLINS, W. E.. 1982. *Proc. International Symposium on the Remote Sensing of the Environment. Second Thematic Mapper Conference. Remote Sensing for Exploration Geology*, Fort Worth, Tx.
- EEV. 1982. CCD imaging. A collection of technical notes prepared by English Electric Valve Ltd., London, England, unpaginated.
- GOEDHEER, J. C. 1972. Fluorescence in relation to photosynthesis. *Ann. Rev. Plant Physiol.* 23: 87-112.
- GORDON, H. R., D. K. CLARK, J. W. BROWN, O. B. BROWN, R. H. EVANS, AND W. W. BROENKOW. 1983. Phytoplankton pigment concentrations in the Middle Atlantic Bight: comparison of ship determinations and CZCS estimates. *Appl. Optics* 22: 20-37.
- GOVINDJEE, G. PAPAGEORGIOU, AND E. RABINOVITCH. 1973. Chlorophyll fluorescence and photosynthesis, p. 543-575. *In* G.G. Guilbault [ed.] *Practical fluorescence, theory, methods and techniques*. Marcel Dekker Inc., New York, NY.
- GOWER, J. F. R.. 1980. Observations of *in situ* fluorescence of chlorophyll *a* in Saanich Inlet. *Boundary Layer Meteorology* 18: 235-245.
1983. FLI noise levels, geometry and spectral observations. Memorandum dated November 10, 1983.
1985. Memorandum concerning FLI noise properties.
- GOWER, J. F. R., AND G. A. BORSTAD. 1981. Use of the *in vivo* fluorescence line at 685nm for remote sensing surveys of surface chlorophyll *a*, p. 329-338. *In* J. F. R. Gower [ed.] *Oceanography from Space*. Plenum Press, New York, NY.
- GOWER, J. F. R., S. LIN, AND G. A. BORSTAD. 1984. The information content of different optical ranges for remote chlorophyll estimation in coastal waters. *Int. J. Remote Sensing* 5: 349-364.
- HODGSON, R. M., F. M. CADY, AND D. PAIRMAN. 1981. A solid state airborne sensing system for remote sensing. *Photogramm. Engineering and Remote Sensing* 47: 177-182.
- HUNT, G. R., J. W. SALISBURY, AND C. J. LENHOFF. 1973. Visible and near infrared spectra of minerals and rocks: VI Additional Silicates. *Mod. Geol.* 4: 85-106.
- ITRES RESEARCH LTD. 1984. Technical improvements and evaluation of the Fluorescence Line Imager sensor. Report prepared by Itres Research Ltd., Calgary for Moniteq Ltd., Concord, Ontario as part of DSS contract serial no. OSB84-00296, November 1984, 25 p.
- JAIN, S. C., H. L. ZWICK, AND R. A. NEVILLE. 1982. An airborne remote sensing and analysis system for water parameters. *International Society for Photogrammetry and Remote Sensing Proceedings. Commission Symposium on Advances in Instrumentation for Processing and Analysis of Photogrammetric and Remotely Sensed Data*. Ottawa.
- KONDRAT'EV, K. YA.. 1973. Radiation characteristics of the atmosphere and the earth's surface. Translation from Russian for NASA and NSF by V. Pandit, Amerind Publishing Co., New Delhi, 580 p.
- LATTIMER, P., AND E. I. RABINOWITCH. 1957. The absolute quantum yields of fluorescence of photosynthetically active pigments. p. 107-112. *In* *Research in Photosynthesis*, Gatlinburg Conference Interscience, New York, NY.
- LIN, S., G. A. BORSTAD, AND J. F. R. GOWER. 1984. Remote sensing of chlorophyll in the red spectral region, p. 137-336. *In* J. C. J. Nihoul [ed], *Remote sensing of shelf sea hydrodynamics*, Elsevier Science Publishers B.V., Amsterdam.
- LYON, R. J. P. 1975. Correlation between ground metal analysis, vegetation reflectance and ERTS brightness over a molybdenum skarn deposit, Pine Nut Mountains, western Nevada. *Proc. 10th Int. Symp. Remote Sensing Environment*. Ann Arbor, Michigan, p. 1031-1044.
- LYZENGA, D. R. 1978. Passive remote sensing techniques for mapping water depth and bottom features, *Appl. Optics* 17: 379-383.
- LYZENGA, D. R., R. A. SHUCHMAN, AND R. A. ARNONE. 1979. Evaluation of an algorithm for mapping bottom features under a depth of water. *Proc. 13th Int. Symp. Remote Sensing Environment*. Ann Arbor, Michigan, p. 1767-1780.
- MCCOLL, W. D., R. A. NEVILLE, AND S. M. TILL. 1983. Multi-detector electro-optical imaging scanner MEIS II. *Proc. 8th Can. Symp. Remote Sensing*, Montreal, Que.
- MONITEQ LTD. 1983. Untitled, undated memorandum concerning spectral dispersion, camera spatial alignments and optical ghost images. Report by Moniteq Ltd., Concord, Ontario for the Department of Fisheries and Oceans, Sidney, B.C.
- 1984a. FLI calibration sphere characterization. Report by Moniteq Ltd. to Department of Fisheries and Oceans, Sidney, B.C., January 1984, 14 p. and appendices.
- 1984b. FLI test and design modification report. Report by Moniteq Ltd. to the Department of Fisheries and Oceans, Sidney, B.C., August 1984, 23 p.
1985. Final report on the technical improvements and evaluation of the Fluorescence Line Imager sensor. Report by Moniteq Ltd., Concord, Ontario for the Department of Fisheries and Oceans, Sidney, B.C., January 1985, 13 p.
- MOREL, A., AND L. PRIEUR. 1977. Analysis of variations in ocean colour. *Limnol. Oceanogr.* 22: 709-722.
- NEVILLE, R. A., AND J. F. R. GOWER. 1977. Passive remote sensing via chlorophyll *a* fluorescence. *J. Geophys. Res.* 82: 343-351.



- NEVILLE, R. A., W. D. MCCOLL, AND S. M. TILL. 1983. Development and evaluation of the MEIS II multi-detector electro-optical imaging sensor. Proceedings of the 1983 SPIE International Technical Conference 395, *Advances in Infrared Sensor Technology*, p. 101-108.
- NORWOOD, V. T., AND J. C. LANSING. 1983. Electro-optical imaging sensors, p. 335-367. *In* R. N. Colwell [ed.] *Manual of Remote Sensing*, 2nd ed., Vol. 1, Am. Soc. Photogrammetry, Falls Church, Virginia.
- SCHMIDT, R.A. 1976. Exploration for porphyry copper deposits in Pakistan using digital processing of Landsat I data. *J. Res. U.S. Geol. Surv.* 4: 27-34.
- SLATER, P. N.. 1980. *Remote sensing, optics and optical systems*. Addison-Wesley Publishing Company, Reading, Massachusetts, 575 p.
- STRICKLAND, J. D. H. AND T. R. PARSONS. 1972. *A practical handbook of seawater analysis*. *Bull. Fish. Res. Board Can.* 167: 130 p.
- THOMPSON, L. L.. 1979. Remote sensing using solid state array technology, *Photogram. Engineering and Remote Sensing* 45: 47-56.
- TILL, S. M., W. D. MCCOLL, AND R. A. NEVILLE. 1983. Development, field performance and evaluation of the MEIS II multi-detector electro-optical imaging scanner. *Proc. 17th Int. Symp. Remote Sensing Environment*, Ann Arbor, Michigan, p. 1137-1146.
- TRACY, R. A., AND R. E. NOLL. 1979. User-oriented data processing considerations in linear array applications. *Photogramm. Engineering and Remote Sensing* 45: 57-61.
- VINCENT, R. K. 1972. An ERTS multispectral scanner experiment for mapping iron compounds. *Proc. 8th Int. Symp. Remote Sensing Environment*, Ann Arbor, Michigan. 4 p.
- WHARTON, S. W., J. R. IRONS, AND F. HUEGEL. 1981. LAPR: an experimental pushbroom scanner. *Photogramm. Engineering and Remote Sensing* 47: 631-639.
- ZWICK, H. H., W. D. MCCOLL, AND H. R. EDEL. 1980. The CCRS DS 1260 Airborne multispectral scanner (MSS). *Proc. 6th Can. Symp. Remote Sensing*, Halifax, p. 643-648.

## APPENDIX — SUMMARY OF THE JUNE AND DECEMBER 1984 TEST FLIGHTS

### A.1. The June 1984 FLI Operations Staged Out of Ottawa

During the week of June 18–22, 1984 a series of three test flights was staged out of Ottawa, Ontario using the CCRS DC-3 aircraft. The purpose of the experiment was to obtain test data from a variety of water and land targets in order to evaluate the performance of the FLI.

The experiment team for this operation consisted of Dr. J. F. R. Gower and Mr. J. S. Wallace of D. F. O. Sidney, Mr. H. Edel of D. F. O. Ottawa; Dr. A. B. Hollinger and Mr. L. Gray of Moniteq Ltd.; and Dr. G. Borstad and Mr. D. Truax of G. A. Borstad Associates Ltd. Supplementary data acquired on the DC-3 aircraft consisted of  $9 \times 9$  colour infra red photographs. Some GNS data was obtained as in-flight notes by Dr. Gower, but no digital data was acquired. Figures A.1 to A.5 illustrate the approximate location of flight lines.

The target for the first flight was a line which had been flown previously by J.F.R. Gower and Moniteq personnel in December 1983. Line 1 over north eastern Lake Ontario was flown four times, three times at 9500' (twice in spatial mode, once in slow spectral mode) and once at 1000' AGL in slow spectral mode. The first two flights were primarily a test of the two types of current controllers, various operating modes and integration times.

Line 2 was a low level, 1000' AGL line in slow spectral mode towards Kingston and over an area in which *in situ* samples were taken by a CCIW (Canada Centre for Inland Waters) vessel on the previous day. Figure A.1 shows the approximate position of the lines.

On June 21, ten lakes in the Eastern Townships just west of Sherbrooke were the target. These lakes have been the subject of intensive studies for several years by the limnology group of McGill University. *In situ* chlorophyll, temperature, secchi transparency and nutrient concentration data were obtained from each lake within 1 or 2 days of our flights. FLI data was obtained over each lake at 1000' AGL in fast spectral mode only. Spatial and slow spectral data obtained over 5 lakes was lost because the HDDT recorder was on but not switched to record. Data obtained late in the mission is affected by patchy cumulus cloud.

Three minutes spatial data was also obtained in the vicinity of west Montreal Island during transit to Ottawa on June 21. This data has not been assigned a line number and no photography was obtained.

On June 22, FLI data was obtained along a line crossing several types of natural and cultivated softwood and hardwood forests near Chalk River, Ontario. Bands were defined according to a request by Dr. D. Leckie, Canadian Forest Service who is now analysing the data himself. The line was flown once in spatial mode and once in fast spectral mode at 9500' AGL, and once in fast spectral mode at 1000' AGL.

Data was also obtained over an agricultural area near Winchester, Ontario on the 22nd in conjunction with  $CO_2$  exchange measurements made by Drs. Mack and des Jardins, Dept. Agriculture, Ottawa. One pass was made in spatial mode at 9500'; two passes (one at 9500', one at 1000') were made in fast spectral mode. Bands used were those defined for lake tests. Skies were clear for both the Petawawa and Winchester flight lines.

TABLE A.1. Spatial mode spectral band definitions for the June and December 1984 test flights.

Band #	June 1984 Excercise		December 1984 Excercise	
	Diode #	Wavelength (nm)	Diode #	Wavelength (nm)
0	2–17	433.7–453.3	28–35	467.7–476.9
1	60–76	509.6–530.5	84–91	540.9–550.1
2	83–99	539.6–560.5	119–126	586.6–595.7
3	155–163	633.5–643.9	155–163	633.5–643.9
4	175–184	659.5–671.2	175–185	659.5–672.5
5	185–192	672.5–681.6	186–196	673.8–686.7
6	242–248	746.2–754.0	213–217	708.8–713.9
7	262–268	772.0–779.7	242–251	746.2–757.8

### A.2. The December 1984 FLI Operations in the Chesapeake Bay area.

During the week of December 10–15, 1984 a series of four joint remote sensing flights involving the Department of Fisheries and Oceans Fluorescence Line Imager (FLI) and the NASA Airborne Oceanographic Lidar (AOL) were flown in the Chesapeake Bay–Cape Hatteras area on the U.S. eastern seaboard (Fig. A6–A.9). All flights were staged out of the NASA Wallops Island Flight Facility approximately 250 km north of Norfolk, Virginia. The purpose of the experiment was to make near simultaneous measurements of solar and laser stimulated *in vivo* chlorophyll fluorescence, in order to compare the two techniques. To this end, the FLI and AOL were flown in two aircraft over the same flight lines within a half hour of one another. Flight lines were chosen to cross several different watermasses, such as the very turbid waters of Pocomoke Sound in Chesapeake Bay, the clearer waters of the open bay itself, the slope waters off the coast and the very clear, blue waters of the Gulf Stream off Cape Hatteras.

The FLI experiment team consisted of two scientists and two technicians plus an aircraft crew of four. The Canadian aircraft (a Falcon fan-jet) carried the Department of Fisheries and Oceans Fluorescence Line Imager, a Daedalus multi-spectral scanner with visible (400–500, 500–550, 600–650, 800–890 nm) and thermal infra-red (8500–14,000 nm) sensors as well as a video-taped television camera for track recovery.

The Canadian research vessel CSS *Hudson* obtained optical and oceanographic samples and profiles (horizontal and vertical) coincident with overflights over Cape Hatteras and the mouth of Chesapeake Bay. These included measurements of *in situ* measurements of active and "passive" solar-stimulated *in vivo* fluorescence.

The AOL experiment team consisted of two scientists and four technicians, an aircraft crew of five and support from NASA Wallops Flight operations and communications personnel. The AOL was being operated with two lasers

TABLE A.2. FLI data from the December 1985 mission on archive at IOS as CCT's, Feb. 1985.

Line #	Altitude (feet)	Nominal ground speed (knots)	Heading (degr)	Mode <sup>a</sup>	Integr. time (ms)	Swath width (km)	IFOV <sup>b</sup> (m)	Image pixel width <sup>c</sup> (m)	Image pixel length <sup>d</sup> (m)	FLI bands stripped	Start time (dddhhmmdd)	Start latitude/longitude (dd,mm/dd,mm)	Tape#
December 13, 1985													
7	500	203	222	2	150	0.2	0.1	4.8	15.7	0	348163124	37,57/75,41	ASO809
8	500	204	183	2	150	0.2	0.1	4.8	15.7	7	348165104	37,33/76,10	ASO810
3	500	204	183	2	150	0.2	0.1	4.8	15.7	7	348165850	37,05/76,08	ASO810
4.1	23,000	428	168	0	90	9.8	6.0	4.6	19.8	0-7	348172900	38,29/76,18	ASO811
4.1	23,000	429	160	0	90	9.8	6.0	4.6	19.8	4,5,6	348172930	38,28/76,18	ASO812
4.2	23,000	420	168	0	90	9.8	6.0	4.6	19.5	4,5,6	348173345	37,59/76,10	ASO813
4.3	23,000	428	168	0	90	9.8	6.0	4.6	19.8	4,5,6	348173800	37,31/76,08	ASO816
4.3	23,000	428	168	0	90	9.8	6.0	4.6	19.8	0-7	348173800	37,31/76,08	ASO834
3	23,000	443	132	0	90	9.8	6.0	4.6	20.5	0-7	348174150	37,05/76,08	ASO815
December 14, 1984													
5a	500	210	195	2	150	0.2	0.1	4.8	16.2	7	349160100	37,12/75,50	ASO803
5a	500	197	170	2	150	0.2	0.1	4.8	15.2	7	349161600	36,27/75,50	ASO803
2	500	203	135	2	150	0.2	0.1	4.8	15.7	7	349162630	35,54/75,35	ASO804
2	31,000	442	133	2	150	13.2	8.1	294.8	34.1	1,4,7	349171452	35,31/75,07	ASO805
2	31,000	325	315	0	90	13.2	8.1	6.1	15.1	0-7	349172200	35,23/75,00	ASO806
2	31,000	328	314	0	90	13.2	8.1	6.1	15.2	0-7	349172330	35,29/75,07	ASO807
U <sup>e</sup>	24,000	403	339	0	90	10.2	6.2	4.8	18.7	0-7	349173800	36,41/76,06	ASO808
December 15, 1984													
9	500	221	90	2	150	0.2	0.1	4.8	17.1	4	350164624	36,54/74,29	ASO818
9	1,500	226	270	2	150	0.6	0.4	14.3	17.5	3	350170821	36,54/73,03	ASO819
9	6,500	260	90	2	150	2.8	1.7	61.8	20.1	4	350173540	36,55/74,16	ASO826
9	13,500	275	269	2	150	5.8	3.5	128.4	21.2	4	350175026	36,55/73,14	ASO827
9	25,000	359	90	2	150	10.7	6.5	237.5	27.7	4	350180713	36,56/74,20	ASO828
9.1	31,000	310	260	0	90	13.2	8.0	6.1	14.4	0-7	350182000	36,56/73,03	ASO829
9.2	31,000	334	270	0	90	13.2	8.0	6.1	15.5	0-7	350182130	36,55/73,04	ASO830
9.3	31,000	337	270	0	90	13.2	8.0	6.1	15.6	0-7	350182300	35,55/74,11	ASO831
9.4	31,000	340	270	0	90	13.2	8.0	6.1	15.8	0-7	350182430	36,55/73,36	ASO832
9.5	31,000	340	270	0	90	13.2	8.0	6.1	15.8	0-7	350182600	36,55/73,47	ASO833

<sup>a</sup>Mode 0 — spatial; Mode 2 — slow spectral.

<sup>b</sup>IFOV — instantaneous field of view for a single array element at nadir (assuming a 0.85 mrad/element).

<sup>c</sup>Pixel width — In spectral mode, only 40 spatial "bands" are read out. For this mission, spectral mode "bands" were 10 elements wide with 38 element gaps between them. Spectral image pixels are therefore 48 × wider (in the cross-track dimension than the 0.65 mrad separation between individual array element centers.

<sup>d</sup>Pixel length = integration time × aircraft velocity.

<sup>e</sup>U — image data acquired on transit over Norfolk, Virginia — no line number.

providing pulsed excitation at 308 and 532 nm. Water colour spectra were obtained from both the laser stimulation and, between pulses, from solar stimulation. Excitation at two wavelengths was intended to allow stimulation of gelbstoffe (308 nm excitation) as well as chlorophyll and phycoerythrin (532 nm excitation). The AOL was flown in a NASA P-3a four engine turbo-prop aircraft, which also carried a Barnes PRT-5 radiometer and a 9 × 9 aerial camera with colour positive film.

The exercise closely followed, but was not coincident with, an oceanographic survey of Chesapeake Bay conducted for the Maryland and Virginia state health authorities December 10–13. This survey consisted of 38 hydrographic stations and some continuous underway sampling between the Bay Bridge-tunnel and Annapolis.

### Chesapeake Bay Exercise: Operational Summary

December 11:

Discussions between scientists and flight operations personnel; detailed flight planning for December 12; instrument and aircraft checkout.

December 12:

Horizontal visibility at low altitude restricted by haze, high scattered cirrus and stratus above.

FLI flight 1: lines 7, 8, and 3 from north to south at 500' altitude in slow spectral mode; attempts to fly line 4 unsuccessful due to military restrictions; line 10 obtained from north to south in spatial mode instead, but at variable altitude under military control. This data will probably not be useful.

AOL flight 1: line 7 aborted due to engine failure.

December 13:

Horizontal visibility at low altitude restricted by haze, scattered cirrus over all of survey area.

FLI flight 2: lines 7, 8 and 3 from north to south at 500' in slow spectral mode; line 4 north to south at 23,000' in spatial mode.

AOL flight 2: lines 7, 8 and 3 north to south at 500' returning along same track.

December 14:

Haze at low altitude, fog and mid-level cloud across the mouth of Chesapeake Bay. Low level cloud near the east end of line 2.

FLI flight 3: line 5a along coast and across the mouth of Chesapeake Bay, over CSS *Hudson* on line 2 off Cape Hatteras, altitude 500' in slow spectral mode; line 2 east to west

at 30,000' in spatial mode; line 2 west to east at 30,000' in slow spectral mode.

AOL flight 3: lines 5a and 2 north to south at 500', returning along the same track.

December 15:

Cloud and fog near the coast, clear over CSS *Hudson* but cloud increasing later in flight.

FLI flight 4: line 9 over CSS *Hudson* at 36°55'N off the mouth of Chesapeake Bay in slow spectral mode at 500', 1500', 6500', 13,500', 25,000' and 31,000' altitude, beginning west to east and alternating direction.

No AOL flight this day.

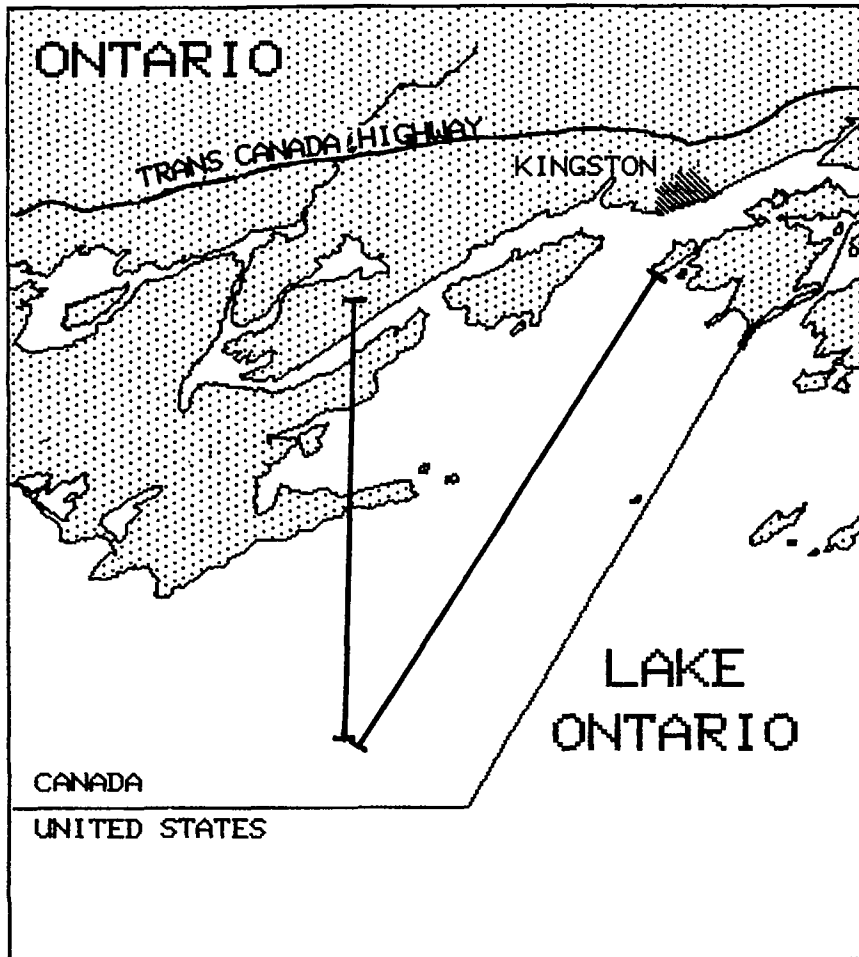


FIG. A.1. Approximate position of lines 1 and 2, flown June 20, 1984 over north eastern Lake Ontario. Spatial and spectral data were obtained at a variety of altitudes and integration times.

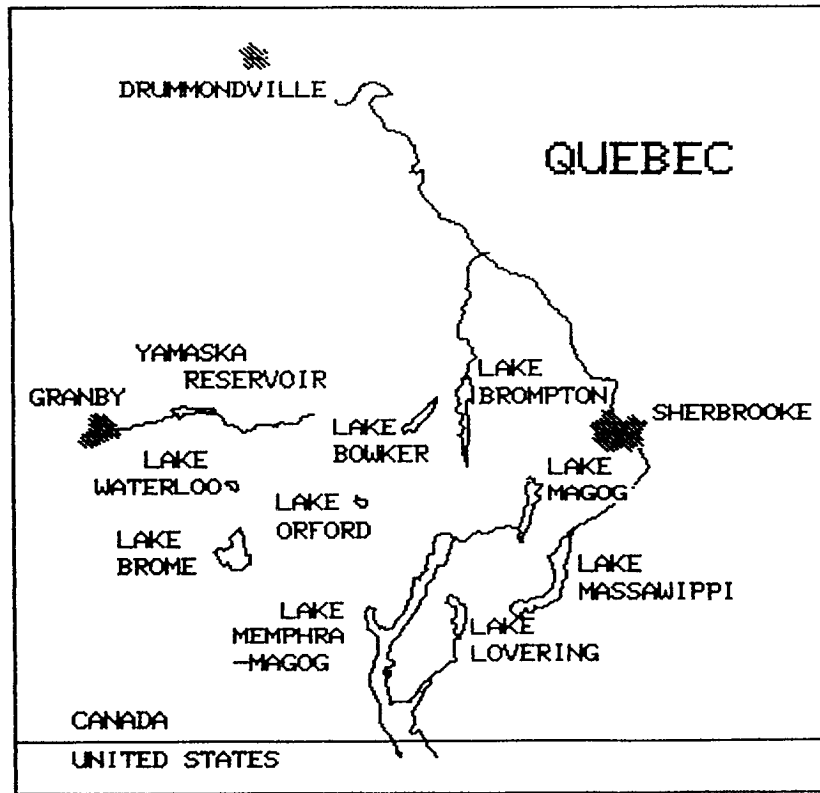


FIG. A.2. Approximate position of lines 3 to 13 and 15 over lakes in the Eastern Townships area of Quebec, June 21, 1984. Fast spectral mode data only, altitude 1000'.

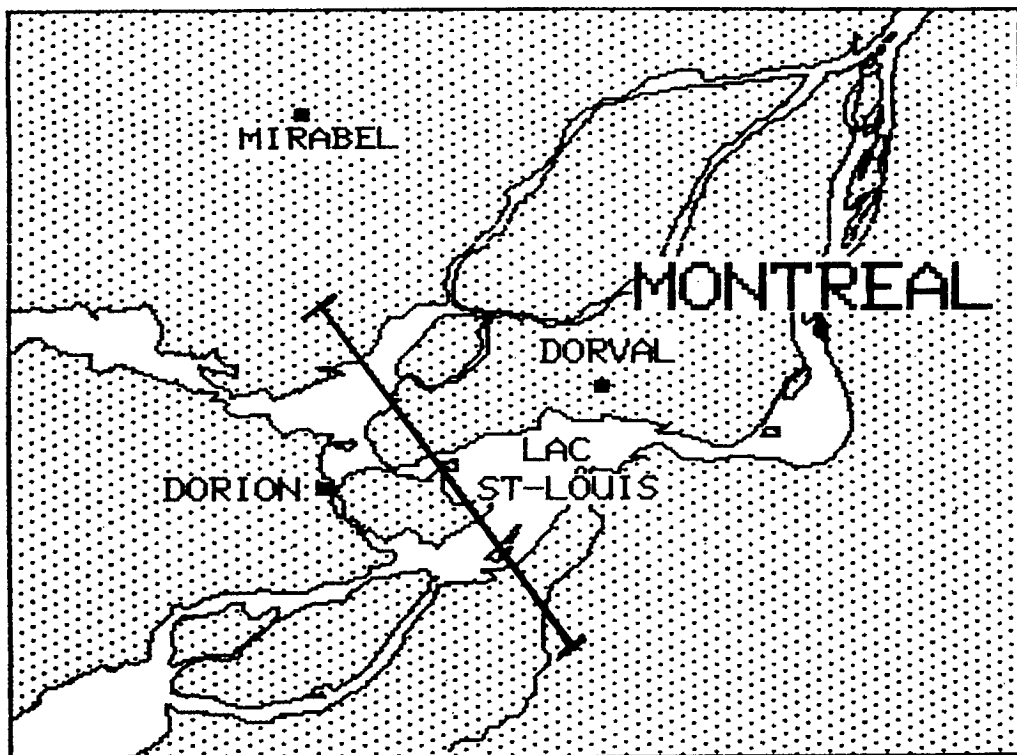


FIG. A.3. Approximate position of spatial mode data obtained June 21, 1984 in transit over the Montreal area (unnumbered line).

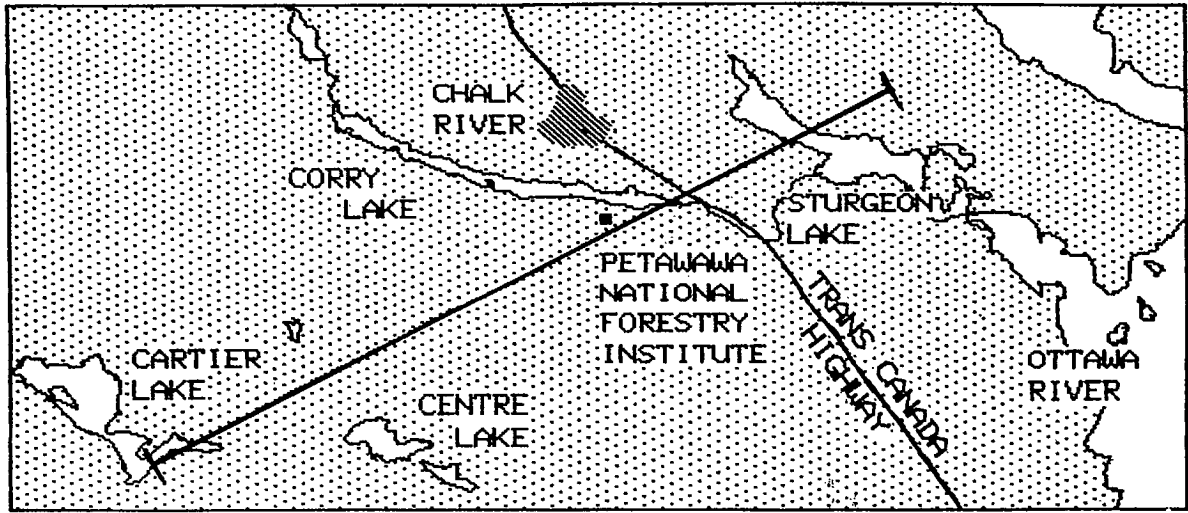


FIG. A.4. Approximate position of line 13 over the Petawawa Experimental Forest area, June 22, 1984. Spatial and spectral data obtained at 9500' and 1000' altitude.

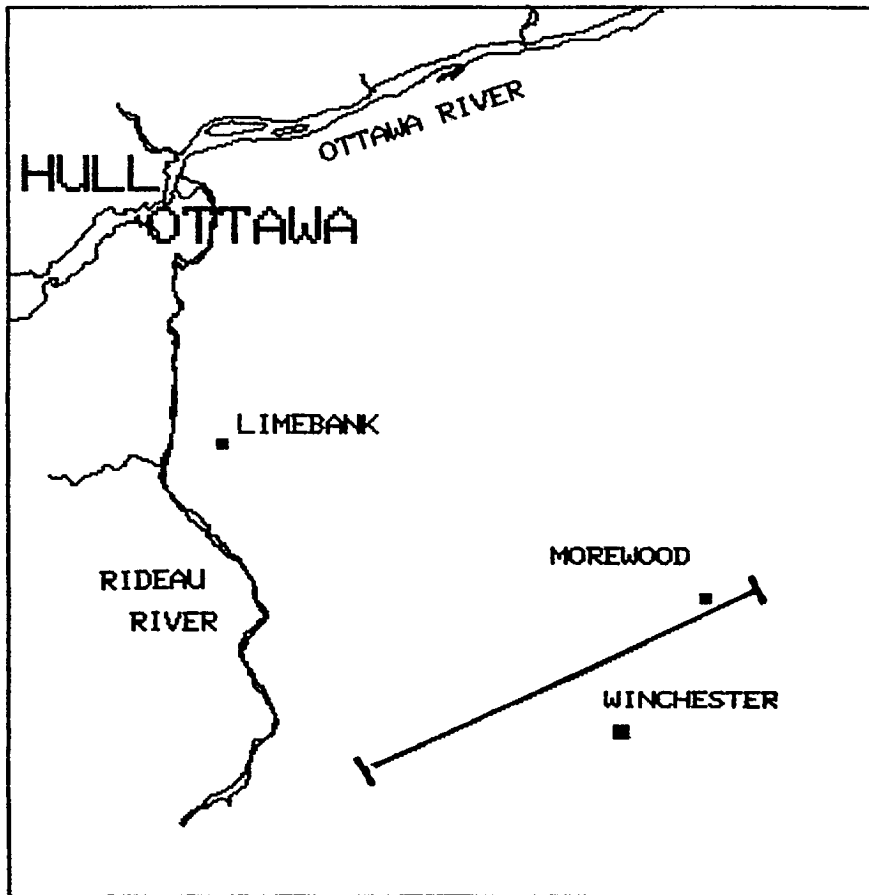


FIG. A.5. Approximate position of line 14 over the Winchester, Ontario agricultural area, June 22, 1984. Spatial and spectral data obtained at 9500' and 1000' altitude.

DATE DUE  
DATE DE RETOUR

Oct 26, 1997			

CANADIAN  
SPACE  
PROGRAM

PROGRAMME  
SPATIAL  
CANADIEN

CSO



Fisheries and Oceans  
Pêches et Océans

Canada